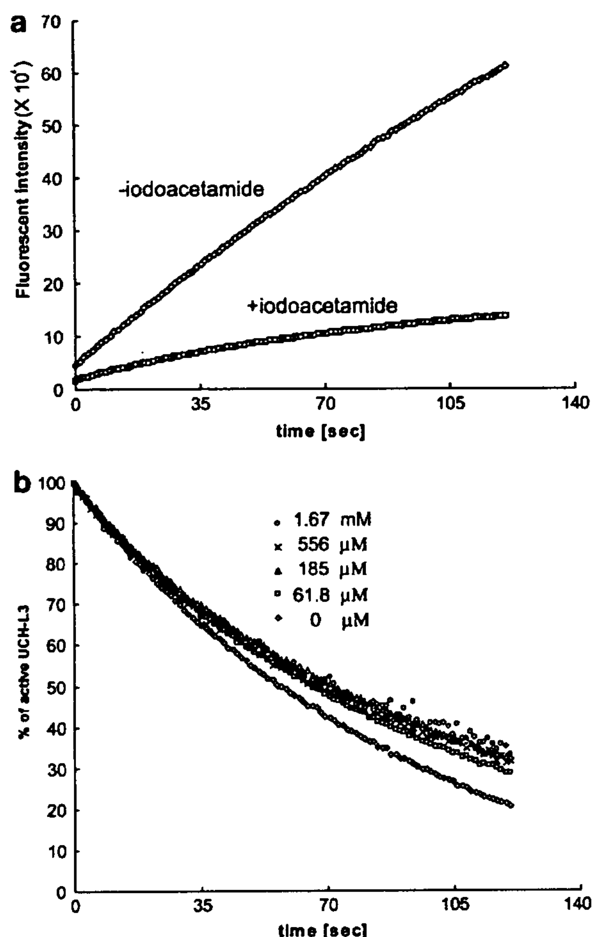

Figure 4. Competitive inhibition of compound 1. (a) Kinetics of UCH-L3-catalyzed hydrolysis of Ub-AMC with or without iodoacetamide (108 mM). (b) Reaction progress curves normalized by final fluorescence intensity representing the ratio of active UCH-L3 (for calculations, see Section 4.9), in the presence of iodoacetamide (108 mM) and compound 1 (0 μM, 61.8 μM, 185 μM, 556 μM, and 1.67 mM).

the pyrrole hydroxyl group and pyrrole C=O appear to form a hydrogen bond to the NH group of Ala11. A hydrogen bond was observed between the docked ligand and the amino acid residues of UCH-L3 in the predicted compound 7/UCH-L3 complex structure; the carbonyl group of compound 7 appears to form a hydrogen bond to the NH group of Ala11. The predicted binding mode of compound 10, as a non-binder, was analyzed. Four hydrogen bonds were observed between the docked ligand and the amino acid residues of UCH-L3 in the predicted compound 10/UCH-L3 complex structure. The triazol group of compound 10 appears to form two hydrogen bonds to the hydroxyl group of Thr157, and the amino group of compound 10 appears to form a hydrogen bond to the CO group of Glu154, and to the CO group of Ser151. Although hydrogen bonds between actual inhibitors (compounds 1, 6, and 7) and Ala11 were observed, compound 10, a non-inhibitor, does not appear to form a hydrogen bond to Ala11. This hydrogen bond might be important for compounds to bind stably to the UCH-L3 active site.

2.6. Discussion; analysis of active compounds

By three-step virtual screening (DOCK, high-speed GOLD, and low-speed GOLD) of 32,799 chemicals, we identified 10 candidate chemicals that potentially inhibit UCH-L3 hydrolysis activity. We examined the actual inhibitory effects of the compounds on UCH-L3 hydrolysis activity by biochemical enzymatic assay and identified three compounds (compounds **1**, **6**, and **7**) as UCH-L3 inhibitors, with IC_{50} values of 100–150 μM. By comparing the structural formulae of the three compounds, we found that the 1,5-dihydro-2*H*-pyrrol-2-one group is likely to be important for inhibition of UCH-L3-hydrolysis activity (Fig. 6). Several common structural features can be drawn from these three chemicals (Fig. 6). First, the heteroaromatic pyrrole group is common to all three compounds. Second, each of the three compounds also contains pyridines and furoyls as heteroaromatic functional groups. Third, a carbon–oxygen double bond at position 2, a hydroxyl group at position 3, a carbonyl group at position 4, and a hydrogen atom at position 5 of the pyrrole ring are common to each compound. Fourth, a five- or six-membered cyclic group at positions 1, 4, and 5 is common to all three chemicals (Fig. 6). Furthermore, compounds **1** and **7** have two heteroaromatic groups: a pyridinyl group and a furoyl group.

The structural similarities of UCH-L3-binding chemicals have an influence on binding mode similarities. There are two main pockets in the substrate-binding site of UCH-L3: the first pocket (Pocket 1) is formed by Pro8, Glu10, and Thr157 and the second pocket (Pocket 2), the active site pocket, is formed by Asp167, Leu168, and Cys90. Docked orientations of compounds **1** and **7** are very similar, as positions 1 and 5 six-membered cyclic groups fit into each pocket. This suggests that two features among these similarities are likely to be important for stable binding to the active site: a pyrrole ring and two heteroaromatic groups, which fit into both pockets around the UCH-L3 substrate-binding site. The shape of Pocket 1 is different from that of UCH-L1,[24] another isoform of the UCH family (52% amino acid sequence identity).[25] Thus, modification of the chemical groups in Pocket 1 might be effective during drug design, to enhance specificity for UCH-L3 over UCH-L1.

Several lines of evidence indicate that UCH-L3 is associated with tumorigenesis and carcinogenesis. High-level expression and activity of UCH-L3 has been reported in multiple types of cancer cells. Expression of UCH-L3 mRNA is upregulated in breast tumors and UCH-L3 mRNA levels are associated with the histological grading of such tumors.[5] Moreover, it has been suggested that the activity of UCH-L3 is also upregulated in the majority of cervical carcinoma tissues, compared with adjacent normal tissues.[6] On the other hand, loss of UCH-L3 is known to induce cell death in knock-out studies. UCH-L3 is involved in the protection of programmed cell death in germ cells and photoreceptor cells in vivo.[7,8] Thus, the structural information of the

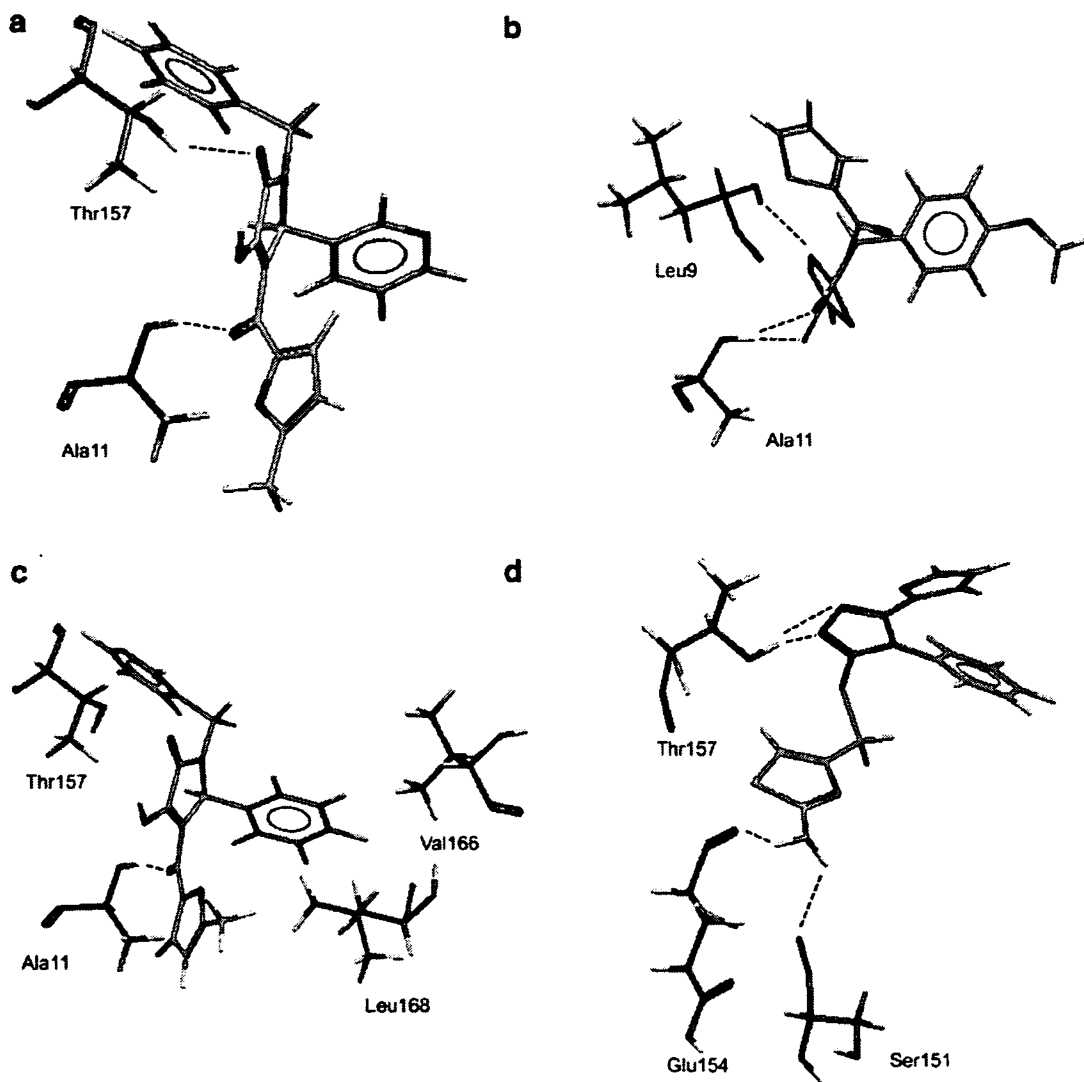

Figure 5. Illustration showing the molecular docking results. Docked orientation of (a) compound **1**, (b) compound **6**, (c) compound **7**, and (d) compound **10** in the UCH-L3 active site using GOLD and shown with interacting residues. Hydrogen bonds are shown by a dashed line. Oxygen atoms are shown in red, nitrogen atoms in blue, sulfur atoms in orange, fluorine atoms in yellow, and hydrogen atoms in gray. The enzyme carbons are shown in dark gray and those of the ligands in green.

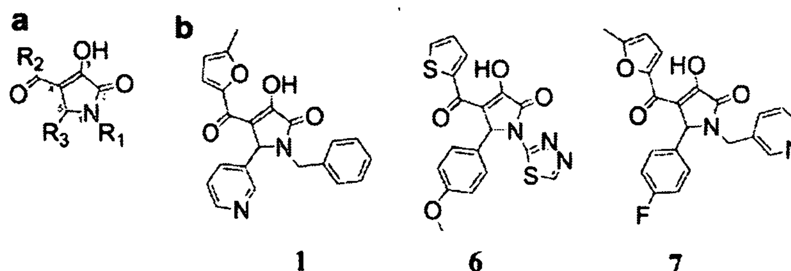

Figure 6. Structural similarities of the three compounds. (a) 1,5-Dihydro-2*H*-pyrrol-2-one group, the common basic skeleton, is shown in red. Position numbers of the pyrrole ring are shown as small characters. R_1–R_3 represent each functional group at positions 1, 4, and 5 of the pyrrole ring, respectively. (b) Structures of identified inhibitors: compounds **1**, **6**, and **7**.

UCH-L3 inhibitors we identified may be useful for future apoptosis-inducing anti-cancer drug development. UCH-L3 should be an important target for modulating cell apoptosis.

3. Conclusion

In this study, we employed three-step docking (DOCK, rough GOLD, and fine GOLD) and in vitro enzyme

assay methods, and identified three UCH-L3 inhibitors with IC_{50} values of 100–150 μM. These novel inhibitors have a dihydro-pyrrole group in common.

4. Experimental

4.1. Compound library

We used the ADME/Tox (absorption, distribution, metabolism, excretion, and toxicity) filtered virtual compound library (ChemBridge CNS-Set) which includes a collection of 32,799 chemical compounds.[18] All compounds satisfy Lipinski's Rule of five.

4.2. Protein preparation

Human UCH-L3 and ubiquitin vinylmethylester (Ub-VME) complex crystal structure data (PDB code; 1XD3) were obtained from Protein Data Bank (PDB).[17] Hydrogens were added to UCH-L3-ubiquitin complex using CVFF99 force field by Biopolymer module in Insight II 2000 suite (Accelrys, Inc., San Diego, CA). Energy was minimized by the Discover 3 module of the same suite with all heavy atoms restrained, except hydrogen, to relieve any short contacts. To use the UCH-L3 protein structure in the following docking simulations, the structures of UCH-L3 and Ub-VME complex were divided into their components.

4.3. Virtual screening

Virtual screening experiments were performed by UCSF DOCK 5.4.0[10] and GOLD 3.0.1 (CCDC, Cambridge, UK).[26] In the first screening by DOCK, the substrate-binding site was defined, by selecting ligand atom accessible spheres and describing molecular surfaces with the SPHERE_GENERATOR program in the DOCK suite. All spheres within 6 Å of root mean square deviation (RMSD) from every atom of the three C-terminal residues of energy-minimized ubiquitin were selected by the SPHERE_SELECTOR program in DOCK suite. A scoring function ($E_{int} = E_{vdw} + E_{elec}$) was used to estimate potential binding affinity. Following the first screening with rigid ligand conditions, 1780 compounds with binding energy scores of less than −30 kcal/mol were selected for a second screening by GOLD.

Using GOLD, the 1780 compounds were screened with 7–8 times speed-up settings; that is, the pre-defined genetic algorithm (GA) parameter settings to achieve calculation speed-up. The top-ranked 100 compounds were determined, then screened by default settings; the GA parameter settings for a slower calculation with greater ligand flexibility, but with a more accurate prediction. Ligand flexibility was turned on in both the 7–8 times speed-up settings and the default settings. Protein side chain flexibility was not turned on in any settings. The virtual tripeptide structure composed of three C-terminal residues of the energy-minimized ubiquitin was set as the reference ligand to define the ligand-binding site. All protein atoms within 5 Å of each ligand atom were used for defining the binding site. The solvent-accessible surfaces of the docking region were restricted by a cavity detection algorithm.[27] As a result, the binding site was composed of 174 active atoms (automatically selected by GOLD software). A method for defining the binding site with tripeptide yielded the best score among other methods using shorter or longer C-terminal peptide sequences of ubiquitin (data not shown). Ten docking solutions for each docked molecule were scored and the top three were saved for post-screening evaluations. Potential hydrogen bonds and van der Waals contacts were identified using Silver 1.0 (CCDC, Cambridge, UK).[28] Ligands predicted to be tight-binders by both DOCK and GOLD were applied to further in vitro experimental validation. All calculations were performed on seven Linux or Cygwin 2–3 GHz/Pentium IV CPU personal computers.

4.4. Statistical analysis

All statistical analysis was performed by GraphPad Prism 4 (GraphPad Software, Inc., San Diego, CA).[29]

4.5. Reagents

Human recombinant UCH-L3, ubiquitin-7-amido-4-methylcoumarin (Ub-AMC), and ubiquitin-aldehyde (Ub-H) were purchased from Boston Biochem, Inc. (Cambridge, MA). 4,5,6,7-Tetrachloroindan-1,3-dione (TCI) was purchased from Fisher Scientific International Inc. (Hampton, NH). Iodoacetamide was purchased from Sigma–Aldrich Corporation (St. Louis, MO). Compounds within ChemBridge CNS-Set (Supplier IDs given in parentheses) are as follows: compound **1**: 1-benzyl-3-hydroxy-4-(5-methyl-2-furoyl)-5-(3-pyridinyl)-1,5-dihydro-2*H*-pyrrol-2-one (7504601); compound **2**: 3-[4-methyl-5-({[3-(2-thienyl)-1,2,4-oxadiazol-5-yl]methyl}thio)-4*H*-1, 2,4-triazol-3-yl]-1*H*-indole (7950509); compound **3**: *N*-{4-[1-(2-furoyl)-5-(2-furyl)-4,5-dihydro-1*H*-pyrazol-3-yl]phenyl}methanesulfonamide (7977303); compound **4**: N^1-cyclopropyl-N^2-(4-methoxyphenyl)-N^2-[(4- methylphenyl)sulfonyl]glycinamide (6382507); compound **5**: *N*-{3-[1-acetyl-5-(2-thienyl)-4,5-dihydro-1*H*-pyrazol-3-yl]phenyl}ethanesulfonamide (7909542); compound **6**: 3-hydroxy-5-(4-methoxyphenyl)-1-(1,3,4-thiadiazol-2-yl)-4-(2-thienylcarbonyl)-1,5-dihydro-2*H*-pyrrol-2-one (6237842); compound **7**: 5-(4-fluorophenyl)-3-hydroxy-4-(5-methyl-2-furoyl)-1-(3-pyridinylmethyl)-1,5-dihydro-2*H*-pyrrol-2-one (6771097); compound **8**: N^1-cyclopropyl-N^2-[(4-methoxyphenyl)sulfonyl]-N^2-(4-methylphenyl)glycinamide (6699002); compound **9**: N^1-cyclopentyl-N^2-(3-methoxyphenyl)-N^2-(phenylsulfonyl)glycinamide (6187162); and compound **10**: 4-({[5-(2-furyl)-4-phenyl-4*H*-1,2,4-triazol-3-yl]thio}methyl)-1,3-thiazol-2-amine (9012750) were purchased from ChemBridge Corporation (San Diego, CA).

4.6. Enzymatic assay

UCH-L3 activity was assayed using modification of a technique described in previous studies.[22,30] The enzyme

reactions were carried out at a final volume of 205 μl on Costar 96-well black assay plates (part number 3915, Corning Inc., Corning, NY). Then, 5 μl of solution containing each compound (100% DMSO), or 5 μl of 100% DMSO as a negative control, was added to 100 μl of enzyme buffer solution (50 pM of UCH-L3, 20 mM Hepes [pH 7.8], 0.5 mM EDTA, 5 mM dithiothreitol [DTT], and 0.1 mg/ml ovalbumin) in each well. The solution was incubated for 30 min at room temperature. To start the enzyme reaction, 100 μl of substrate buffer solution (82 nM of ubiquitin-AMC, 20 mM Hepes [pH 7.8], 0.5 mM EDTA, 5 mM DTT, and 0.1 mg/ml ovalbumin) was added to each well. AMC fluorescence (excitation wavelength: 355 nm, emission wavelength: 460 nm) was subsequently measured 40 times every 3 s with a Wallac 1420 multi-label counter (Perkin-Elmer, Wellesley, MA).

4.7. K_m determination

Fifty microliters of enzyme buffer solution was added to each plate well. The solution was incubated for 30 min at room temperature. To start the enzyme reaction, 50 μl of substrate buffer solution (23.1, 46.3, 92.5, 185, 370, and 740 nM of ubiquitin-AMC; the concentrations of other components were as described previously) was added to each well. Fluorescence of AMC was measured 40 times every 3 s with the Wallac multi-label counter. Initial velocities (from 0 to 30 s) were used for K_m determination, using GraphPad Prism 4 software.[29]

4.8. Experimental IC_{50} determination

Five microliters of solution containing each compound (0.412 μM, 1.23, 3.70, 11.1, 20, 33.3, 50, 100, 300, and 700–850 μM) or 5 μl of 100% DMSO (as a negative control) diluted in 100 μl of enzyme buffer solution was added to each plate well. This solution was incubated for 30 min at room temperature. To start the enzyme reaction, 100 μl of substrate buffer solution was added to each well. Fluorescence of AMC was measured 40 times every 3 s with the Wallac multi-label counter. Initial velocities (from 0 to 30 s) were used for IC_{50} determination, using GraphPad Prism 4 software.[29]

4.9. Active site binding experiment

Modification of a technique described in previous studies was used to determine whether or not the compounds bind to the active site.[22] Five microliters of solution containing compound 1 (0 μM, 61.8 μM, 185 μM, 556 μM, and 1.67 mM) or 5 μl of 100% DMSO (as a negative control) diluted in 80 μl of enzyme buffer solution (UCH-L3: 1 nM) was added to each plate well. This solution was incubated for 30 min at room temperature. To start the enzyme reaction, 80 μl of substrate buffer solution (Ub-AMC: 1 μM) was added to each well, followed within 2 s by addition of 40 μl of iodoacetamide (108 mM) or water as a negative control. Fluorescence of AMC was measured 100 times every second using the Wallac multi-label counter. The percentage of active site survival $[(F_{\text{saturated}} - F_t)/(F_{\text{saturated}} - F_{t=0}) \times 100]$ was calculated.

Acknowledgments

This work was supported by Grants-in-Aid for Scientific Research from the Ministry of Health, Labour and Welfare of Japan, Grants-in-Aid for Scientific Research from the Ministry of Education, Culture, Sports, Science and Technology of Japan, a grant from the Program for Promotion of Fundamental Studies in Health Sciences of the National Institute of Biomedical Innovation, a grant from Japan Science and Technology Cooperation, and a grant from New Energy and Industrial Technology Development Organization. We thank Takashi Kaburagi for demonstrating how to set up the DOCK software.

References and notes

1. Ciechanover, A.; Schwartz, A. L. *Proc. Natl. Acad. Sci. U.S.A.* **1998**, *95*, 2727–2730.
2. Pickart, C. M.; Rose, I. A. *J. Biol. Chem.* **1985**, *260*, 7903–7910.
3. Waldmeier, P.; Bozyczko-Coyne, D.; Williams, M.; Vaught, J. L. *Biochem. Pharmacol.* **2006**, *72*, 1197–1206.
4. Aktas, O.; Waiczies, S.; Zipp, F. *J. Neuroimmunol.* **2007**, *184*, 17–26.
5. Miyoshi, Y.; Nakayama, S.; Torikoshi, Y.; Tanaka, S.; Ishihara, H.; Taguchi, T.; Tamaki, Y.; Noguchi, S. *Cancer Sci.* **2006**, *97*, 523–529.
6. Rolen, U.; Kobzeva, V.; Gasparjan, N.; Ovaa, H.; Winberg, G.; Kisseljov, F.; Masucci, M. G. *Mol. Carcinog.* **2006**, *45*, 260–269.
7. Kwon, J.; Wang, Y. L.; Setsuie, R.; Sekiguchi, S.; Sato, Y.; Sakurai, M.; Noda, M.; Aoki, S.; Yoshikawa, Y.; Wada, K. *Am. J. Pathol.* **2004**, *165*, 1367–1374.
8. Sano, Y.; Furuta, A.; Setsuie, R.; Kikuchi, H.; Wang, Y. L.; Sakurai, M.; Kwon, J.; Noda, M.; Wada, K. *Am. J. Pathol.* **2006**, *169*, 132–141.
9. Kuntz, I. D.; Blaney, J. M.; Oatley, S. J.; Langridge, R.; Ferrin, T. E. *J. Mol. Biol.* **1982**, *161*, 269–288.
10. Ewing, T. J.; Makino, S.; Skillman, A. G.; Kuntz, I. D. *J. Comput. Aided Mol. Des.* **2001**, *15*, 411–428.
11. FlexX, BioSolveIT GmbH, Sankt Augustin, Germany, <http://www.biosolveit.de/>.
12. Peng, H.; Huang, N.; Qi, J.; Xie, P.; Xu, C.; Wang, J.; Yang, C. *Bioorg. Med. Chem. Lett.* **2003**, *13*, 3693–3699.
13. McNally, V. A.; Gbaj, A.; Douglas, K. T.; Stratford, I. J.; Jaffar, M.; Freeman, S.; Bryce, R. A. *Bioorg. Med. Chem. Lett.* **2003**, *13*, 3705–3709.
14. Olsen, L.; Jost, S.; Adolph, H. W.; Pettersson, I.; Hemmingsen, L.; Jorgensen, F. S. *Bioorg. Med. Chem.* **2006**, *14*, 2627–2635.
15. Miteva, M. A.; Lee, W. H.; Montes, M. O.; Villoutreix, B. O. *J. Med. Chem.* **2005**, *48*, 6012–6022.
16. Johnston, S. C.; Larsen, C. N.; Cook, W. J.; Wilkinson, K. D.; Hill, C. P. *EMBO J.* **1997**, *16*, 3787–3796.
17. Misaghi, S.; Galardy, P. J.; Meester, W. J.; Ovaa, H.; Ploegh, H. L.; Gaudet, R. *J. Biol. Chem.* **2005**, *280*, 1512–1520.
18. RPBS, Paris, France, <http://bioserv.rpbs.jussieu.fr/RPBS/cgi-bin/Ressource.cgi?chzn_lg=an&chzn_rsrc=Collections/>.
19. GOLD User Guide, 16.2.1, CCDC, Cambridge, UK, <http://www.ccdc.cam.ac.uk/support/documentation/gold/3_1/gold31.pdf/>.
20. Dang, L. C.; Melandri, F. D.; Stein, R. L. *Biochemistry* **1998**, *37*, 1868–1879.

21. Mason, D. E.; Ek, J.; Peters, E. C.; Harris, J. L. *Biochemistry* **2004**, *43*, 6535–6544.
22. Liu, Y.; Lashuel, H. A.; Choi, S.; Xing, X.; Case, A.; Ni, J.; Yeh, L. A.; Cuny, G. D.; Stein, R. L.; Lansbury, P. T., Jr. *Chem. Biol.* **2003**, *10*, 837–846.
23. Stenlund, P.; Frostell-Karlsson, A.; Karlsson, O. P. *Anal. Biochem.* **2006**, *353*, 217–225.
24. Das, C.; Hoang, Q. Q.; Kreinbring, C. A.; Luchansky, S. J.; Meray, R. K.; Ray, S. S.; Lansbury, P. T.; Ringe, D.; Petsko, G. A. *Proc. Natl. Acad. Sci. U.S.A.* **2006**, *103*, 4675–4680.
25. Kurihara, L. J.; Semenova, E.; Levorse, J. M.; Tilghman, S. M. *Mol. Cell. Biol.* **2000**, *20*, 2498–2504.
26. Jones, G.; Willett, P.; Glen, R. C.; Leach, A. R.; Taylor, R. *J. Mol. Biol.* **1997**, *267*, 727–748.
27. Hendlich, M.; Rippmann, F.; Barnickel, G. *J. Mol. Graph. Model.* **1997**, *15*, 359–363.
28. Silver, CCDC, Cambridge, UK, <http://www.ccdc.cam.ac.uk/>.
29. GraphPad Prism 4, GraphPad Software, San Diego, CA, <http://www.graphpad.com/www/about.htm/>.
30. Nishikawa, K.; Li, H.; Kawamura, R.; Osaka, H.; Wang, Y. L.; Hara, Y.; Hirokawa, T.; Manago, Y.; Amano, T.; Noda, M.; Aoki, S.; Wada, K. *Biochem. Biophys. Res. Commun.* **2003**, *304*, 176–183.

ELSEVIER

Available online at www.sciencedirect.com

ScienceDirect

European Journal of Pharmacology 573 (2007) 20–28

ejp

www.elsevier.com/locate/ejphar

Alpha 1-adrenoceptor agonists protect against stress-induced death of neural progenitor cells

Hiroki Ohashi [a,b], Kaori Nishikawa [a,c], Koichi Ayukawa [a,d], Yoko Hara [a], Mika Nishimoto [a,e], Yoshihisa Kudo [e], Toshiaki Abe [b], Shunsuke Aoki [a,c,f,*], Keiji Wada [a,f]

[a] *Department of Degenerative Neurological Diseases, National Institute of Neuroscience, NCNP, Kodaira, Tokyo 187-8502, Japan*
[b] *Department of Neurosurgery, Jikei University Graduate School of Medicine, Minatoku, Tokyo 105-8401, Japan*
[c] *NEDO (New Energy and Industrial Technology Development Organization), Kawasaki, Kanagawa 212-8554, Japan*
[d] *Japan Society for the Promotion of Science (JSPS), Chiyodaku, Tokyo 102-8471, Japan*
[e] *Laboratory of Cellular Neurobiology, Tokyo University of Pharmacy and Life Science, Hachioji, Tokyo 192-0392, Japan*
[f] *CREST (Core Research for Evolutional Science and Technology) of Japan Science and Technology Corporation (JST), Kawaguchi, Saitama 332-0012, Japan*

Received 15 February 2007; received in revised form 18 June 2007; accepted 26 June 2007
Available online 12 July 2007

Abstract

Here, we show that α_1-adrenoceptor agonists suppress stress-induced death of mouse embryonic brain-derived neural progenitor cells (NPCs). NPCs highly expressed both α_{1A}- and α_{1B}-adrenoceptor genes, whereas the gene encoding α_{1D}-adrenoceptor was expressed at low levels. Application of the α_1-adrenoceptor agonists phenylephrine and cirazoline significantly promoted cell survival of embryonic NPCs that had been exposed to stress, as measured by a lactate dehydrogenase release assay, but had no remarkable effect on differentiation of the NPCs. Both phenylephrine and cirazoline protected NPCs from death induced by growth factor deprivation, N2 nutrient deprivation, tunicamycin treatment or staurosporine treatment. Phenylephrine and cirazoline treatments both maximally reduced stress-induced cell death by ~60% but did not change the percentage of undifferentiated cells as measured by nestin staining. Moreover, phenylephrine and cirazoline treatments did not affect the cellular activities of caspase-3 and caspase-7 but markedly reduced propidium iodide penetration into the cytoplasm, suggesting that α_1-adrenoceptor agonists inhibit caspase-3/7-independent death of the embryonic NPCs.
© 2007 Elsevier B.V. All rights reserved.

Keywords: α_1-adrenoceptor; GPCR; Neural progenitor cell; Cell death; Cell stress; Phenylephrine; Cirazoline

1. Introduction

The noradrenergic system is proposed to play multiple roles in the adult central nervous system (CNS). Apart from its classical transmitter signaling action, noradrenaline has important roles in attention, arousal, and memory reviewed in Murchison et al., (2004); Southwick et al., (1999). Furthermore, it was proposed that noradrenaline influences the survival, maintenance and plasticity of CNS neurons, including the regulation of endogenous neurotrophin systems, glial function, CNS energy utilization and extracellular homeostasis, and has anti-inflammatory and anti-oxidant effects reviewed in Marien et al., (2004). All cell surface adrenoceptors are members of the G protein-coupled receptor family and mediate responses to extracellular noradrenaline. To date, three subfamilies of adrenoceptors (α_1, α_2 and β) have been identified (Bylund et al., 1995). The adrenoceptors are expressed in many tissues, particularly in the cardiovascular, genitourinary and nervous systems. High levels of adrenoceptors are also present in the neocortex during embryogenesis (Lidow and Rakic, 1992), and there are regional concentrations of α_1, α_2, and β adrenoceptors in the fetal forebrain (Lidow and Rakic, 1994). There are three subtypes of α_1-adrenoceptors, the α_{1A}, α_{1B}, α_{1D}-adrenoceptor, with varying degrees of efficiency of G protein (Gq/11) coupling ($\alpha_{1A}>\alpha_{1B}>\alpha_{1D}$ adrenoceptor) reviewed in Hieble et al., (1995). This leads to activation of downstream signal

* Corresponding author. Department of Degenerative Neurological Diseases, National Institute of Neuroscience, National Center of Neurology and Psychiatry, 4-1-1 Ogawahigashi, Kodaira, Tokyo 187-8502, Japan. Tel.: +81 42 346 1715; fax: +81 42 346 1745.
E-mail address: aokis@ncnp.go.jp (S. Aoki).

0014-2999/$ - see front matter © 2007 Elsevier B.V. All rights reserved.
doi:10.1016/j.ejphar.2007.06.060

transduction pathways, including Ca^{2+}, arachidonic acid, phospholipase C and phospholipase D signals reviewed in Zhong and Minneman (1999). α_1-adrenoceptors are specifically localized to NPCs located in the ventricular zone and subventricular zone in the embryonic rat forebrain, and noradrenaline-containing fibers are also present in both the ventricular zone and subventricular zone (Pabbathi et al., 1997). In addition, noradrenaline has been suggested to regulate development of the murine forebrain. The β-adrenoceptor agonist isoproterenol alters proliferation and differentiation of neural precursors in the cerebral cortex (Slotkin et al., 1988). α_1-adrenoceptors were also implicated in controlling cell proliferation and survival in a rat cortical mixed cell culture and in a heterochronic coculture system of the rat neocortex and rostral pons (Pabbathi et al., 1997; Popovik and Haynes, 2000). Although the functions of α_1-adrenoceptors in the mixed-culture NPCs and in the organ culture were investigated, the function of α_1-adrenoceptors and the direct effects of α_1-adrenoceptor-selective agonists such as phenylephrine and cirazoline in isolated pure embryonic NPCs are not known.

The precise role of the α_1-adrenoceptor-mediated signal in embryonic cortical NPCs remains obscure, because the effects observed in the mixed-cell and organ culture experiments possibly reflect the secondary and tertiary effects mediated by multiple cellular interactions (glial cell-progenitor, neuronal cell-progenitor and neuronal cell-glial cell-progenitor interactions). As such, the aim of this study is to know the primary biological effect of α_1-adrenoceptor activation in the NPCs. We addressed the biological effects of α_1-adrenoceptor-selective agonists on highly purified embryonic NPCs. Our data indicate that these agonists inhibit death of NPCs cultured under various stress conditions but do not affect proliferation, differentiation or caspase-3/7-activity.

2. Materials and methods

2.1. Animals

Pregnant C57BL/6J mice were purchased from CLEA Japan (Tokyo, Japan). Animal care and handling were in accordance with institutional regulations for animal care and public law, and were approved by the Animal Investigation Committee of the National Institute of Neuroscience, Japan.

2.2. Antibodies and reagents

Monoclonal and polyclonal antibodies used in this study were as follows: monoclonal anti-nestin (Becton Dickinson, Lexington, KY), monoclonal anti-tuj1 (Covance, Berkeley, CA), polyclonal anti-glial fibrillary acidic protein (Dako, Carpinteria, CA), monoclonal anti-galactocerebroside (Chemicon International, Temecula, CA). The secondary antibodies conjugated to Alexa Fluor dye were purchased from Molecular Probes (Eugene, OR). α_1-adrenoceptor agonists used in this study were (*R*)-3-[1-hydroxy-2-(methylamino) ethyl] phenol (phenylephrine; Sigma, St. Louis, MO) and 2-[(2-cyclopropylphenoxy) methyl]-4, 5-dihydro-1H-imidazole (cirazoline; Tocris, Ellisville, MO). Each agonist was dissolved in Neurobasal™ medium (Invitrogen, Carlsbad, CA). Staurosporine and tunicamycin (Sigma) were dissolved in dimethyl sulfoxide (DMSO). Each solution was added to the medium, and the final concentration of DMSO in the medium was adjusted to at most 0.1% (v/v). Medium containing the same amount of organic solvent was used as a negative control.

2.3. Cortical NPCs culture

Cortical NPCs were cultured as previously described (Fukazawa et al., 2006). Briefly, embryos were removed from pregnant C57BL/6J mice and were staged according to morphological criteria to confirm gestational age. Developing mouse brain and cerebral cortex containing the ventricular and subventricular zones were dissected from embryonic day 14 (E14) embryos. Cells were mechanically dissociated by trituration and plated at 3.0×10^6 cells per 10-cm dish (BD) precoated with 15 μg/ml poly-L-ornithine (Sigma) and 1 μg/ml fibronectin (Nitta Gelatin, Osaka, Japan). Cells were expanded for 4 days in serum-free Neurobasal medium supplemented with 0.5 mM L-glutamine (Invitrogen), 100 U/ml penicillin, 100 μg/ml streptomycin (Invitrogen) and B27 (biotin, L-carnitine, corticosterone, ethanolamine, D(+)-galactose, glutathione (reduced), linoleic acid, linolenic acid, progesterone, putrescine, retinyl acetate, selenium, T3 (triodo-l-thyronine), DL-α-tocopherol (vitamin E), DL-α-tocopherol acetate, bovine serum albumin, catalase, insulin, superoxide dismutase, transferrin, vitamin A (Brewer et al., 1993); Invitrogen). N2 supplement (100 mg/l apo-transferrin, 5 mg/l insulin, 16 mg/l putrescine, 6.3 μg/l progesterone, 5 μg/l selenite; Sigma) were used for stress experiments instead of the B27 supplement. This medium was supplemented with 10 ng/ml basic fibroblast growth factor (bFGF; PeproTech, Rocky Hill, NJ) except when mentioned otherwise. Cultures were maintained at 37 °C in an atmosphere of 95% air and 5% CO_2. For secondary cultures, bFGF-expanded cortical NPCs were washed in warm Hanks' balanced salt solution, detached with mechanically pipetting, and resuspended in Neurobasal medium. Cells were then re-seeded on 24-well plates (Nunc; 1.8×10^5 cells/well), or 48-well plates (Nunc; 1.5×10^5 cells/well) precoated with poly-L-ornithine and fibronectin.

2.4. Real-time quantitative reverse-transcription (RT)-PCR

Real-time quantitative RT-PCR with the SYBR Green-based detection method was performed as previously described (Aoki et al., 2002). Total RNA was isolated from cultured cortical NPCs and E14 mouse cerebral cortex. These RNAs (1 μg) were treated with DNase I and converted to cDNA with Superscript II reverse transcriptase (Invitrogen) and random hexamer primers according to the manufacturer's instructions. The efficiency of reverse transcription and the quality of cDNA was compared with the efficiency of PCR amplification of the hypoxanthine guanine phosphoribosyl transferase (hprt) gene (GenBank accession ID. NM_013556; forward primer, 5′-TCTTTGCTGACCTGCTGGATT-3′; reverse primer, 5′-TATGTCCCCCGTTGACTGATC-

3′). Primers were designed for the α_{1A} (NM_013461), α_{1B} (NM_007416) and α_{1D} (NM_013460) adrenoceptor genes using Primer Express software (Perkin-Elmer, Torrance, CA). The forward and reverse primer sequences were as follows: 5′-TTT-CAAGCCACCGGAAACA-3′ and 5′-ACTGGATTCGCAGCA-CATTCT-3′ (α_{1A}); 5′-AACCCTTCTACGCCCTCTTTTC-3′ and 5′-CCAGATTCTTGGTGGTCCTCTT-3′ (α_{1B}); and 5′-TCG-CTCAAGTATCCAGCCATT-3′ and 5′-AACCTAG-TAGCGGTCCCACAGA-3′ (α_{1D}). SYBR Green-based real-time RT-PCR was performed in 12.5-μl reactions (ABI PRISM 7700 Sequence Detection System, Perkin-Elmer). PCR products were analyzed with agarose gel electrophoresis. We checked each primer individually to ensure that the primer was selective for the target (data not shown). We also ensured that no band was observed in gel electrophoresis of PCRs that included distilled water or total RNA preparation without reverse transcriptase as template. The quantitative RT-PCR method (User Bulletin #2, Applied Biosystems, Foster City, CA) was modified to establish an expression level index for mRNA (Aoki et al., 2002), and the SYBR Green signal for the hprt amplicon was used as a reference. Amplification efficiency was determined and confirmed in a control PCR experiment using serial cDNA dilutions as templates. The real-time RT-PCR products were analyzed using the Applied Biosystems sequence detection system software 1.7.

2.5. LDH and ATP assay

The number of non-viable cortical NPCs was quantitatively assayed by measuring the activity of the cytosolic enzyme lactate dehydrogenase (LDH) released into the culture medium after membrane rupture. LDH activity was measured using the cytotoxicity assay CytoTox-ONE™ Homogeneous Membrane Integrity Assay (Promega, Madison, WI). To quantify the number of viable cells in cultured cortical NPCs, the amount of cellular ATP was measured using the CellTiter-Glo™ Luminescent Cell Viability Assay (Promega). These assays were performed in accordance with the manufacturer's protocol and on secondary cultured cortical NPCs as described above. Four hundred μl (1.5×10^5 cells/well) of cell suspension was added to each well of a 48-well plate (Nunc) precoated with poly-L-ornithine and fibronectin. After 24 h, cells were treated without or with 10 μM phenylephrine or cirazoline with different concentrations of bFGF or under different stress conditions as described in the figure legends. Cultures were then returned to the 37 °C incubator for 24 h, and assessment of LDH release in the media and amount of ATP was conducted with a Wallac 1420 multilabel counter (Perkin-Elmer, Finland).

2.6. Immunocytochemistry

Cells were stained as we have previously described with minor modifications (Sakurai et al., 2006). Briefly, all incubations and washes were performed at room temperature. Cells were fixed with 3.8% formaldehyde in phosphate-buffered saline (PBS) for 10 min and permeabilized with 0.02% (w/v) Triton X-100 in PBS for 5 min. Fixed cells were blocked with 3.3% goat serum in PBS for 30 min. Cells were incubated for 30 min with anti-nestin (neural progenitor marker; 1:500), anti-tuj1 (early neuronal cell marker; 1:500)(Sakurai et al., 2006), anti-glial fibrillary acidic protein (astrocyte marker; 1:1000) or anti-galactocerebroside (immature oligodendrocyte marker; 1:200)(Fukazawa et al., 2006). These cells were incubated with diluted secondary antibody (1:200) conjugated to Alexa Fluor for 30 min. All primary and secondary antibodies were diluted in 1% goat serum in PBS before use. The fluorescence microscopy images were obtained with an IX70 microscope (Olympus).

2.7. Quantification of enzymatic activities of caspases

Caspase-3 and caspase-7 protease activities were determined using the Caspase-Glo™ 3/7 Assay kit (Promega). All assays were performed on secondary cultured cortical NPCs as described above. Four hundred μl (1.5×10^5 cells/well) of cell suspension was added to each well of a 48-well plate (Nunc) precoated with poly-L-ornithine and fibronectin. After 24 h, cells were treated with or without 10 μM phenylephrine in medium lacking the N2 supplement as described in the figure legends. Cultures were then returned to the 37 °C incubator for 24 h, and caspase-3 and -7 activities were assessed with a Wallac 1420 multilabel counter.

2.8. Measurement of cell death using propidium iodide

All assays were performed on secondary cultured cortical NPCs as described above. Four hundred μl (1.5×10^5 cells/well) of cell suspension was added to each well of a 48-well plate (Nunc) precoated with poly-L-ornithine and fibronectin. After 24 h, cells were treated with or without 10 μM phenylephrine in medium lacking the N2 supplement. Cultures were then returned to the 37 °C incubator and maintained for 24 h, then stained with 1 μg/ml propidium iodide. Only dead cells with permeable plasma membranes were stained with propidium iodide. Positive controls were stained with propidium iodide after fixing with 3.8% formaldehyde in PBS for 10 min and permeabilized with 0.02% Triton X-100 in PBS. Dead cells and positive controls stained with propidium iodide were counted by fluorometry (Wallac 1420 multilabel counter).

2.9. Statistical analysis

Results are expressed as the mean±standard error of the mean (S.E.M.). Either the Student's *t*-test or Dunnett's multiple range test was used to evaluate the data using Prism software version 4.03 (GraphPad, San Diego, CA). Values of $P<0.01$ and $P<0.05$ were considered statistically significant depending on the specific experiment.

3. Results

3.1. Embryonic cortical NPCs express α_1-adrenoeceptor genes

We analyzed gene expression levels of the three α_1-adrenoceptors, and all were expressed both in the E14 embryonic

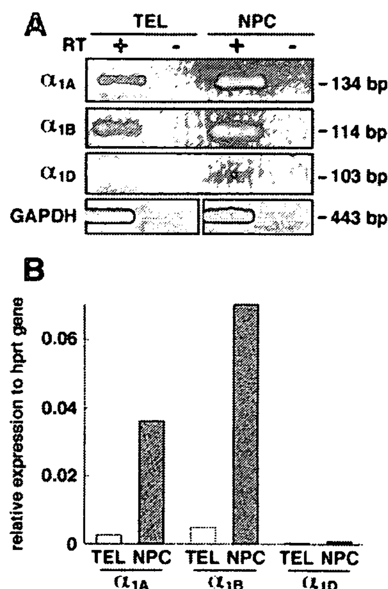

Fig. 1. NPCs derived from E14 telencephalon express α_{1A}-adrenoceptor (α_{1A}), α_{1B}-adrenoceptor (α_{1B}) and α_{1D}-adrenoceptor (α_{1D}). Total RNA isolated from cultured NPCs and E14 mouse telencephalon (TEL) was reverse-transcribed, and the resultant cDNA was used in RT-PCR analysis. (A) As indicated on the left, the PCR products corresponding to the α_{1A}, α_{1B}, and α_{1D} adrenoceptor genes and *GAPDH* were separated on a 3% agarose gel. The size of PCR products are indicated on the right. (B) Gene expression levels of the α_{1A}, α_{1B} and α_{1D} adrenoceptor were analyzed by quantitative RT-PCR, and the expression levels relative to *hprt* are presented. The results are representative of three separate experiments that yielded similar results.

telencephalon and E14 telencephalon-derived cultured NPCs (Fig. 1A). Semi-quantitative analysis of expression levels of the α_1-adrenoceptor genes (normalized to the internal control, *hprt*) showed that the isolated NPCs highly expressed α_{1A}, α_{1B} and α_{1D} adrenoceptor genes as compared with the E14 telencephalon (Fig. 1B). Among the α_1-adrenoceptor genes, the α_{1A} and α_{1B} genes were highly expressed in the cultured NPCs, whereas a low level of expression was detected for the α_{1D} gene in both the E14 telencephalon and cultured NPCs (Fig. 1B).

3.2. Effect of the α_1-adrenoceptor agonist phenylephrine on NPC differentiation

E14 telencephalon-derived NPCs have potencies to differentiate into multiple neural cell types, including neurons, astrocytes and oligodendrocytes, in the absence of bFGF (Fig. 2). The effect of phenylephrine, an α_1-adrenoceptor-selective agonist, on NPC differentiation was examined using the neural cell differentiation marker tuj1 for neuronal cells, glial fibrillary acidic protein for astroglial cells and galactocerebroside for oligodendrocytes. At 72 h after bFGF deprivation, 41.8±1.0% of the NPCs had differentiated into tuj1-positive ($tuj1^+$) cells, 40.6±6.0% of the NPCs had differentiated into glial fibrillary acidic protein-positive ($GFAP^+$) cells and 9.4±1.1% were galactocerebroside-positive (GC^+) (Fig. 2A and B). Phenylephrine treatment did not significantly change the percentages of neuronal and glial cells ($tuj1^+$, 38.1±3.2%; $GFAP^+$, 28.7±3.1%; and GC^+, 6.2±1.0%) in cultures lacking bFGF (Fig. 2A and B). These results indicate that phenylephrine did not affect NPC differentiation induced by bFGF deprivation. We also examined the effect of phenylephrine on neural differentiation of NPCs in cultures containing bFGF and again found no effect on neuronal or glial differentiation (data not shown).

3.3. α_1-adrenoceptor agonists protect NPCs from cell death

It has been reported that activation of α_1-adrenoceptors stimulates DNA synthesis of embryonic NPCs in mixed culture conditions (Pabbathi et al., 1997). Primary NPC cultures prepared from the telencephalon contain a considerable number of neuronal cells (>10%) that also express α_1-adrenoceptors (Papay et al., 2006). To determine whether the previously reported activation of DNA synthesis was indicative of NPC proliferation or proliferation by secondary effect via other cell types contaminating the culture, we re-seeded cultured NPCs from a primary culture to prepare highly purified secondary

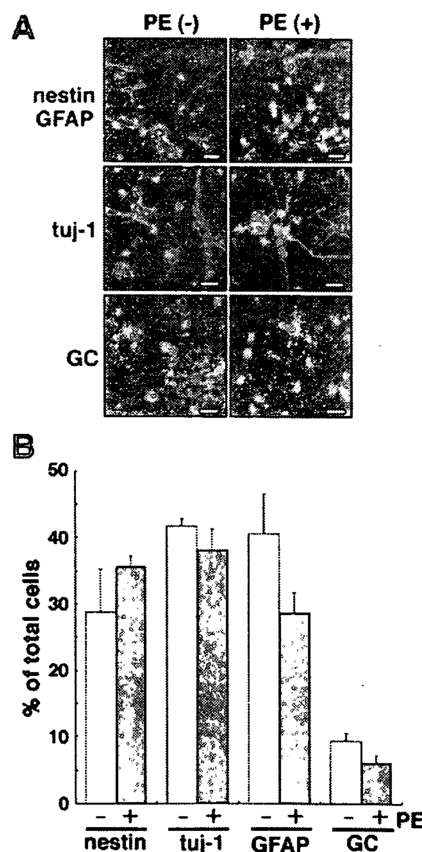

Fig. 2. Effect of the α_1-adrenoceptor agonist phenylephrine on NPC differentiation. (A) Immunofluorescence staining was carried out after 72 h on NPC cultures with or without phenylephrine. Fluorescence microscopic images of cells labeled with anti-nestin (green), anti-GFAP (red), anti-tuj1 (green) and anti-galactocerebroside (green) are shown; nuclei are stained with Hoechst (blue). Scale bar = 20 μm. Similar results were obtained in two independent experiments. (B) Secondary cultured NPCs from the E14 mouse telencephalon were maintained *in vitro* for 72 h without or with 10 μM phenylephrine (PE). After 72 h, cells were fixed and immunostained for tuj1, glial fibrillary acidic protein (GFAP), nestin and galactocerebroside (GC). The number of $nestin^+$, $tuj1^+$, $GFAP^+$ and GC^+ cells were counted, and the percentages are presented. Nestin was used as a marker for undifferentiated NPCs. No significant differences were observed.

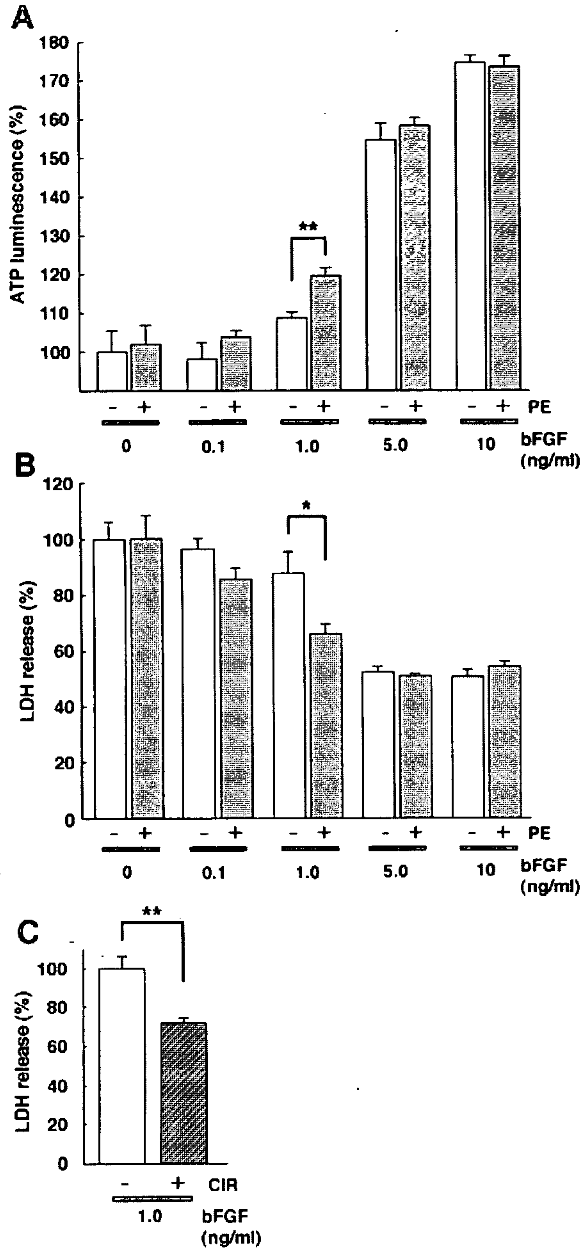

Fig. 3. Effects of α_1-adrenoceptor agonists on the number of cells and cell death of NPCs at various doses of bFGF. Secondary cultured NPCs from the E14 mouse telencephalon were treated without or with 10 μM phenylephrine at different concentrations of bFGF for 24 h. (A) The number of NPCs was examined with an ATP luminescence assay. (B) The viability of NPCs was examined with the LDH release assay. (C) Secondary cultured NPCs from the E14 mouse telencephalon were treated without or with 10 μM cirazoline in 1 ng/ml bFGF for 24 h. Cell survival was assessed by the ATP luminescence assay. Bars represent mean±S.E.M. (n=4). Significant differences are indicated by single or double asterisks (*$P<0.05$, **$P<0.01$, Student's t-test).

NPC cultures that contained over 99±0.4% nestin$^+$ undifferentiated NPCs and no more than 0.5% tuj1$^+$ neuronal cells. Using the secondary NPC culture, we examined whether phenylephrine increased the number of NPCs at various doses of bFGF (0 ~ 10 ng/ml) using an intracellular ATP luminescence assay (Crouch et al., 1993; Petty et al., 1995). We found that phenylephrine significantly increased the number of NPCs only at a moderate dose (1.0 ng/ml) of bFGF ($P<0.01$; Fig. 3A) and had no significant effect at high doses (5–10 ng/ml), a low dose (0.1 ng/ml) of bFGF, or no bFGF. To determine whether the effect of phenylephrine on NPCs at 1 ng/ml bFGF was due to promotion of cell growth or cell survival, we examine the effect of phenylephrine on cell death using the LDH release assay (Decker and Lohmann-Matthes, 1988), which measures destruction of the plasma membrane. Phenylephrine also significantly decreased LDH release at 1 ng/ml bFGF ($P<0.05$; Fig. 3B), indicating that the difference between ATP luminescence (cell numbers) of phenylephrine-treated and

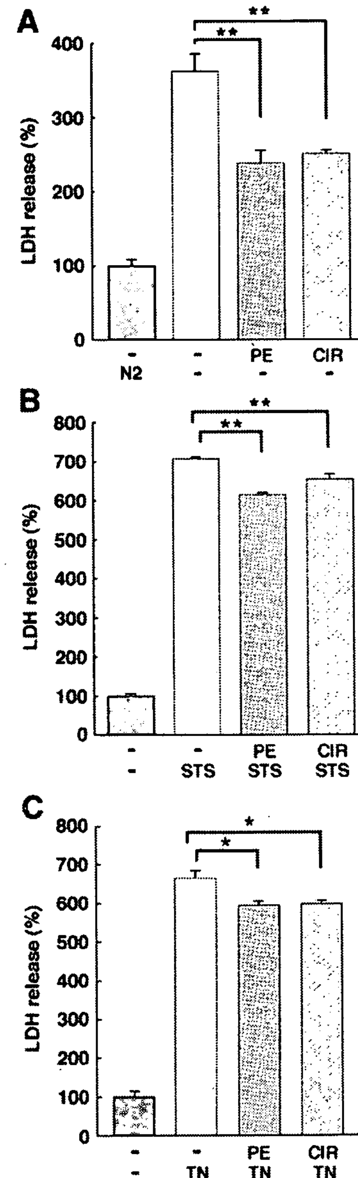

Fig. 4. Phenylephrine and cirazoline promote survival of NPCs under various stress conditions. Secondary cultured NPCs from the E14 mouse telencephalon were incubated in medium lacking N2 (A), 50 nM staurosporine (STS) (B) or 30 ng/ml tunicamycin (TN) (C) in the presence or absence of 10 μM phenylephrine (PE) or 10 μM cirazoline (CIR) for 24 h. Quantification of cell death was performed with the LDH release assay. Bars represent mean±S.E.M. (n=3 ~ 5). Significant differences are indicated by single or double asterisks (*$P<0.05$, **$P<0.01$, Dunnett's test).

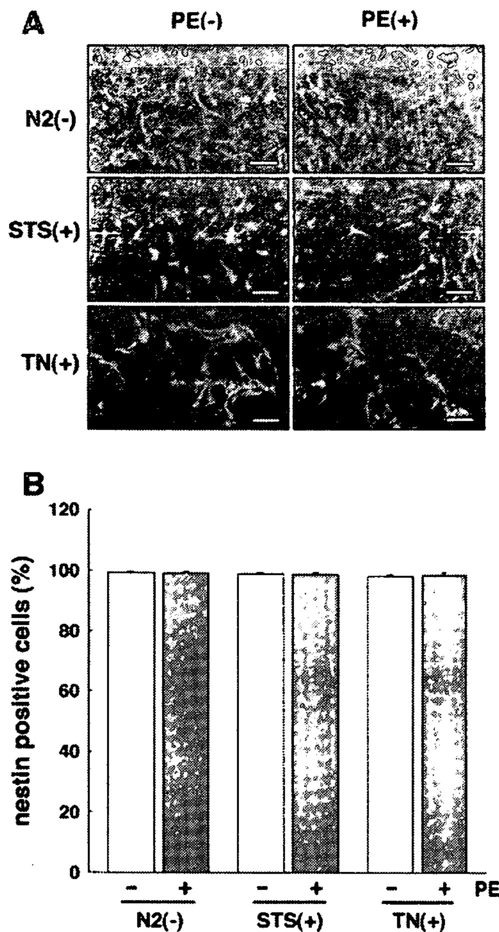

Fig. 5. Effect of phenylephrine on the proportion of nestin-positive cells under various stress conditions. Secondary cultured NPCs were exposed for 24 h to stress conditions without or with 10 μM phenylephrine: N2 deprivation medium, or exposure to 50 nM staurosporine (STS) or 30 ng/ml tunicamycin (TN). After 24 h, the NPCs were fixed and stained with anti-nestin and Hoechst. (A) Fluorescence microscopic images of cells labeled with anti-nestin (green) and Hoechst (blue). Scale bar = 50 μm. (B) The percentages of nestin-positive cells in the cultures were quantified. No significant differences were seen among the groups.

untreated NPCs correlated with the difference in the amount of cell death. These results also indicated that phenylephrine protected NPCs from death during bFGF deprivation-induced stress. Moreover, we confirmed that α_1-adrenoceptor agonists specifically protected NPCs from death using another α_1-adrenoceptor agonist, cirazoline. Cirazoline treatment of NPCs under the same culture conditions resulted in a significant decrease in LDH release ($P<0.01$; Fig. 3C), indicating that α_1-adrenoceptor agonists promote survival of NPCs cultured in 1 ng/ml bFGF. A [^{3}H]thymidine incorporation assay showed that phenylephrine and cirazoline did not induce DNA synthesis of NPCs (data not shown).

3.4. α_1-adrenoceptor agonists prevent NPC death upon exposure to various stresses

To determine the extent to which α_1-adrenoceptor agonists could prevent NPC death, we employed other stress conditions: N2 deprivation, or exposure to 50 nM staurosporine or 30 ng/ml tunicamycin. The results of the LDH release assay for these stress conditions showed that N2 deprivation, staurosporine treatment, and tunicamycin treatment induced LDH release from NPCs (361±24%, 706±5% and 664±21%, respectively, relative to the controls; Fig. 4). However, application of the agonists to the NPC cultures under these stress conditions significantly reduced LDH release (N2 deprivation+phenylephrine, 238±18% $P<0.01$; N2

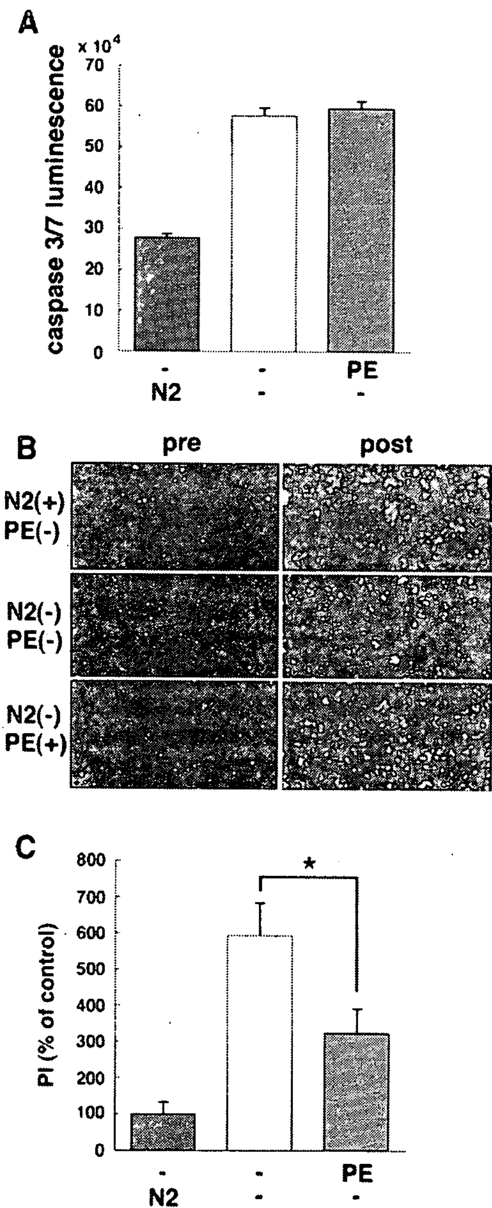

Fig. 6. Phenylephrine does not alter cellular caspase activity but changes propidium iodide penetration into NPCs. Secondary cultured NPCs were incubated without or with 10 μM phenylephrine (PE) under N2 deprivation conditions for 24 h. (A) Caspase-3 and caspase-7 activities in cell lysates were measured by luminometry. (B) Fluorescence microscopy images of dead cells stained with propidium iodide are presented (left). For positive controls, cells were fixed and stained with PI after permeabilization with 0.02% Triton X-100 (right). Scale bar = 100 μm. (C) The intensity of propidium iodide staining was measured by fluorometry. Bars represent mean±S.E.M. ($n=4$). Significant differences are indicated by an asterisk (*$P<0.05$, Dunnett's test).

deprivation+cirazoline, 251±5% $P<0.01$; staurosporine+phenylephrine, 614±9% $P<0.01$; staurosporine+cirazoline, 654±16% $P<0.01$; and tunicamycin+phenylephrine, 594±13% $P<0.05$; tunicamycin+cirazoline, 597±10% $P<0.05$) (Fig. 4). Under the three stress conditions, the differences in the efficacies of phenylephrine and cirazoline on LDH release did not differ greatly. However, both agonists were most effective against N2 deprivation stress, where phenylephrine and cirazoline reduced LDH release 34% and 31%, respectively, as compared with the unstressed control (Fig. 4A). These data suggest that α_1-adrenoceptor agonists protected NPC death under several different stress conditions but exhibited different efficacies depending on the particular stress.

3.5. α_1-adrenoceptor agonists do not modulate the proportion of nestin-positive NPCs under stress conditions

Phenylephrine did not affect differentiation of NPCs in cultures with or without bFGF (Fig. 1), and the high proportion (over 98%) of nestin-positive cells remained for ~24 h even in 1 ng/ml bFGF (data not shown). The ability of the agonists to prevent cell death in 1 ng/ml bFGF was thus a direct effect on the nestin-positive NPCs and not an artifact due to contaminating cells. We also examined the effects of stress induced by N2 deprivation, 50 nM staurosporine or 30 ng/ml tunicamycin on NPC differentiation to exclude the possibility that the increased cell numbers observed following α_1-adrenoceptor agonist exposure, as measured by ATP production, were derived from the differentiated cells induced by the stresses. The proportion of nestin-positive NPCs was not changed by N2 deprivation, staurosporine-or tunicamycin-induced stress, and treatment of NPCs with phenylephrine or cirazoline under these stress conditions did not decrease the proportions of nestin-positive cells (Fig. 5).

3.6. Phenylephrine inhibits caspase-3/7-independent cell death

Of the three stress conditions tested, α_1-adrenoceptor agonists most effectively suppressed stress caused by N2 deprivation, as measured by LDH release (Figs. 3 and 4). Whereas cell death induced by bFGF deprivation, staurosporine treatment or tunicamycin treatment probably was caused by activation of various death signaling pathways, the stress caused by N2 deprivation mainly induced caspase-3/7-dependent cell death in NPC cultures (Fig. 6). To ascertain whether α_1-adrenoceptor agonists protect against caspase-3/7-dependent cell death, we examined the effects of α_1-adrenoceptor agonists on cellular caspase-3/7 activities. Stress caused by N2 deprivation induced elevated cellular caspase-3 and caspase-7 activities as compared with non-stress conditions (>2 fold; Fig. 6A). However, the elevated activities of caspases were not changed by treatment of NPCs with phenylephrine (Fig. 6A). Despite a lack of modulation of the cellular caspase activity, phenylephrine suppressed propidium iodide penetration into NPC cytoplasm (45.4%; $P<0.05$, as compared with untreated cells deprived of N2) (Fig. 6B and C). These data indicate that α_1-adrenoceptor agonists selectively protect against caspase-3/7-independent death of NPCs exposed to stress.

4. Discussion

In this study, we prepared highly purified embryonic NPCs (>99% nestin$^+$ cells) from the E14 mouse cortex and found that the cortical embryonic NPCs highly express α_{1A}- and α_{1B}-adrenoceptor genes but express the α_{1D}-adrenoceptor gene at low levels. Our pharmacological experiments also revealed that α_1-adrenoceptor agonists are protective against NPC death induced by various stresses without any modification of the cell differentiation state of the NPCs. Moreover we demonstrated that α_1-adrenoceptor agonists reduced NPC death caused by the N2 deprivation stress without modulation of intracellular caspase-3/7 activities.

The α_1-adrenoceptor is expressed in the ventricular zone and subventricular zone of the embryonic rat forebrain (Pabbathi et al., 1997). The ventricular zone of the embryonic cerebral cortex contains both undifferentiated NPCs and differentiated nascent neuronal cells. Our quantitative RT-PCR analysis showed that purified cortical NPCs express α_{1A}- and α_{1B}-adrenoceptor genes at high levels compared with the E14 embryonic telencephalon, suggesting that the undifferentiated NPCs highly expressed the α_{1A}- and α_{1B}-adrenoceptor genes. We could not confirm the expression of α_1-adrenoceptor proteins in NPCs because of low specificity of commercially available antibodies against α_1-adrenoceptor in immunocytochemical experiments with NPCs (data not shown). However, we demonstrated that α_1-adrenoceptor agonists have protective effects against cell death in NPCs, indicating the presence of the α_1-adrenoceptors in NPCs.

The chemical structure of phenylephrine ((*R*)-3-[1-hydroxy-2-(methylamino) ethyl] phenol) differs from that of cirazoline (2-[(2-cyclopropylphenoxy) methyl]-4, 5-dihydro-1H-imidazole). However, both α_1-adrenoceptor agonists had the same effect on NPC death induced by a moderate concentration (1 ng/ml) of bFGF, nutritional deprivation (no N2 supplementation), staurosporine treatment or endoplasmic reticulum stress (tunicamycin treatment), indicating that the effects were specifically mediated by α_1-adrenoceptors. It is well known that cell death can be induced via multiple apoptosis signaling pathways that are specifically activated by different stresses. Although the α_1-adrenoceptor agonists were able to protect NPCs from death induced by the stresses we tested, the molecular mechanism that underlies this broad protection is unknown. However, treatment of NPCs with α_1-adrenoceptor agonists failed to decrease the activities of caspase-3 and caspase-7, which are activated in the apoptosis pathway. Instead, α_1-adrenoceptor agonists reduced propidium iodide incorporation induced by stress caused by N2 deprivation. These data suggest that α_1-adrenoceptor agonists protect against necrotic NPC death but not apoptotic NPC death.

Phenylephrine or cirazoline protects against cell death induced by bFGF deprivation as well as by STS and nutritional deprivation, or treatment with staurosporine or tunicamycin. Niidome et al. (Niidome et al., 2006) showed that NPC death resulting from growth factor deprivation is caused by both caspase-dependent and -independent pathways in concert with oxidative stress, suggesting that α_1-adrenoreceptor agonists may also protect against NPC death induced by oxidative stresses. On the other hand, application of phenylephrine is effective only against cell death induced by 1.0 ng/ml bFGF. Complete

deprivation of growth factors activates multiple cell death pathways, including apoptosis, necrosis and the oxidative cell death pathway, in cultured NPCs (Niidome et al., 2006). Therefore, the application of phenylephrine is unlikely to be effective against NPC death induced by the overlapping activation of multiple death pathways after complete loss of growth factor support.

In a recent study, Hiramoto et al. (2006) reported that the stimulation of α_1-adrenoreceptors by phenylephrine or by L-epinephrine induces the proliferation of NPCs derived from cultured neurospheres. Our data indicate that α_1-adrenoreceptor agonists do not induce proliferation of purified NPCs. It is known that the neurospheres have the 3D organization in which nestin-positive (progenitor) cells surround a large core of differentiated GFAP-positive (glial) and β-tubulin III-positive (neuronal) cells (Campos, 2004). As such, the NPC cultures prepared from neurospheres could also contain glial and neuronal cells. Thus, the difference between these data may have resulted from differences in the NPC preparation methods and from the purity of the nestin-positive NPCs.

Transplantation of neural stem and progenitor cells into patients with intractable neurological diseases is considered an effective strategy for neural regeneration therapy reviewed in Lindvall et al., (2004). Studies on cell transplantation/implantation for CNS disorders have indicated that neural stem cells and progenitor cells have the ability to replace lost neurons and to repair the damaged nervous system (Chu et al., 2004). However, a large proportion of grafted cells is lost due to early necrotic death. Thus, the low rate of graft survival reduces the effectiveness of such therapies (Emgard et al., 2003). Here we demonstrated that α_1-adrenoceptor agonists protect against NPC death (probably necrotic death) induced by various stresses. We also demonstrated that α_1-adrenoceptor agonists with this protective effect did not modify the cell differentiation state of the NPCs. Thus, α_1-adrenoceptor agonists may be useful for the preparation and maintenance of neural stem and progenitor cells for transplantation therapy, as they are likely to increase cell viability without induction of unexpected cell differentiation. Moreover, phenylephrine is a popular and safe drug that is used as a non-prescription decongestant (Chua and Benrimoj, 1988) Therefore, phenylephrine may be easily applied as an additional reagent in the cultivation medium of neural stem and progenitor cells for transplantation therapy.

Acknowledgments

This work was supported in part by Grants-in-Aid for Scientific Research from the Ministry of Health, Labour and Welfare of Japan, Grants-in-Aid for Scientific Research from the Ministry of Education, Culture, Sports, Science and Technology of Japan, the Program for Promotion of Fundamental Studies in Health Sciences of the National Institute of Biomedical Innovation, and a grant from Japan Science and Technology Agency.

References

Aoki, S., Su, Q., Li, H., Nishikawa, K., Ayukawa, K., Hara, Y., Namikawa, K., Kiryu-Seo, S., Kiyama, H., Wada, K., 2002. Identification of an axotomy-induced glycosylated protein, AIGP1, possibly involved in cell death triggered by endoplasmic reticulum-Golgi stress. J. Neurosci. 22, 10751–10760.

Brewer, G.J., Torricelli, J.R., Evege, E.K., Price, P.J., 1993. Optimized survival of hippocampal neurons in B27-supplemented neurobasal, a new serum-free medium combination. J. Neurosci. Res. 35, 567–576.

Bylund, D.B., Regan, J.W., Faber, J.E., Hieble, J.P., Triggle, C.R., Ruffolo Jr., R.R., 1995. Vascular alpha-adrenoceptors: from the gene to the human. Can. J. Physiol. Pharm. 73, 533–543.

Campos, L.S., 2004. Neurospheres: insights into neural stem cell biology. J. Neurosci. Res. 78, 761–769.

Chu, K., Kim, M., Jung, K.H., Jeon, D., Lee, S.T., Kim, J., Jeong, S.W., Kim, S.U., Lee, S.K., Shin, H.S., Roh, J.K., 2004. Human neural stem cell transplantation reduces spontaneous recurrent seizures following pilocarpine-induced status epilepticus in adult rats. Brain Res. 1023, 213–221.

Chua, S.S., Benrimoj, S.I., 1988. Non-prescription sympathomimetic agents and hypertension. Med. Toxicol. Adverse Drug Exp. 3, 387–417.

Crouch, S.P., Kozlowski, R., Slater, K.J., Fletcher, J., 1993. The use of ATP bioluminescence as a measure of cell proliferation and cytotoxicity. J. Immunol. Methods 160, 81–88.

Decker, T., Lohmann-Matthes, M.L., 1988. A quick and simple method for the quantitation of lactate dehydrogenase release in measurements of cellular cytotoxicity and tumor necrosis factor (TNF) activity. J. Immunol. Methods 115, 61–69.

Emgard, M., Hallin, U., Karlsson, J., Bahr, B.A., Brundin, P., Blomgren, K., 2003. Both apoptosis and necrosis occur early after intracerebral grafting of ventral mesencephalic tissue: a role for protease activation. J. Neurochem. 86, 1223–1232.

Fukazawa, N., Ayukawa, K., Nishikawa, K., Ohashi, H., Ichihara, N., Hikawa, Y., Abe, T., Kudo, Y., Kiyama, H., Wada, K., Aoki, S., 2006. Identification and functional characterization of mouse TPO1 as a myelin membrane protein. Brain Res. 1070, 1–14.

Hieble, J.P., Bondinell, W.E., Ruffolo Jr., R.R., 1995. Alpha- and beta-adrenoceptors: from the gene to the clinic. 1. Molecular biology and adrenoceptor subclassification. J. Med. Chem. 38, 3415–3444.

Hiramoto, T., Ihara, Y., Watanabe, Y., 2006. Alpha-1 Adrenergic receptors stimulation induces the proliferation of neural progenitor cells in vitro. Neurosci. Lett. 408, 25–28.

Lidow, M.S., Rakic, P., 1992. Scheduling of monoaminergic neurotransmitter receptor expression in the primate neocortex during postnatal development. Cereb. Cortex 2, 401–416.

Lidow, M.S., Rakic, P., 1994. Unique profiles of the alpha 1-, alpha 2-, and beta-adrenergic receptors in the developing cortical plate and transient embryonic zones of the rhesus monkey. J. Neurosci. 14, 4064–4078.

Lindvall, O., Kokaia, Z., Martinez-Serrano, A., 2004. Stem cell therapy for human neurodegenerative disorders—how to make it work. Nat. Med. (10 Suppl), S42–S50.

Marien, M.R., Colpaert, F.C., Rosenquist, A.C., 2004. Noradrenergic mechanisms in neurodegenerative diseases: a theory. Brain Res. Brain Res. Rev. 45, 38–78.

Murchison, C.F., Zhang, X.Y., Zhang, W.P., Ouyang, M., Lee, A., Thomas, S.A., 2004. A distinct role for norepinephrine in memory retrieval. Cell 117, 131–143.

Niidome, T., Morimoto, N., Iijima, S., Akaike, A., Kihara, T., Sugimoto, H., 2006. Mechanisms of cell death of neural progenitor cells caused by trophic support deprivation. Eur. J. Pharmacol. 548, 1–8.

Pabbathi, V.K., Brennan, H., Muxworthy, A., Gill, L., Holmes, F.E., Vignes, M., Haynes, L.W., 1997. Catecholaminergic regulation of proliferation and survival in rat forebrain paraventricular germinal cells. Brain Res. 760, 22–33.

Papay, R., Gaivin, R., Jha, A., McCune, D.F., McGrath, J.C., Rodrigo, M.C., Simpson, P.C., Doze, V.A., Perez, D.M., 2006. Localization of the mouse alpha1A-adrenergic receptor (AR) in the brain: alpha1AAR is expressed in neurons, GABAergic interneurons, and NG2 oligodendrocyte progenitors. J. Comp. Neurol. 497, 209–222.

Petty, R.D., Sutherland, L.A., Hunter, E.M., Cree, I.A., 1995. Comparison of MTT and ATP-based assays for the measurement of viable cell number. J. Biolumin. Chemilumin. 10, 29–34.

Popovik, E., Haynes, L.W., 2000. Survival and mitogenesis of neuroepithelial cells are influenced by noradrenergic but not cholinergic innervation in cultured embryonic rat neopallium. Brain Res. 853, 227–235.

Sakurai, M., Ayukawa, K., Setsuie, R., Nishikawa, K., Hara, Y., Ohashi, H., Nishimoto, M., Abe, T., Kudo, Y., Sekiguchi, M., Sato, Y., Aoki, S., Noda, M., Wada, K., 2006. Ubiquitin C-terminal hydrolase L1 regulates the morphology of neural progenitor cells and modulates their differentiation. J. Cell Sci. 119, 162–171.

Slotkin, T.A., Windh, R., Whitmore, W.L., Seidler, F.J., 1988. Adrenergic control of DNA synthesis in developing rat brain regions: effects of intracisternal administration of isoproterenol. Brain Res. Bull. 21, 737–740.

Southwick, S.M., Bremner, J.D., Rasmusson, A., Morgan 3rd, C.A., Arnsten, A., Charney, D.S., 1999. Role of norepinephrine in the pathophysiology and treatment of posttraumatic stress disorder. Biol. Psychiatry 46, 1192–1204.

Zhong, H., Minneman, K.P., 1999. Alpha1-adrenoceptor subtypes. Eur. J. Pharmacol. 375, 261–276.

European Journal of Neuroscience, Vol. 27, pp. 691–701, 2008 doi:10.1111/j.1460-9568.2008.06047.x

Reduction in memory in passive avoidance learning, exploratory behaviour and synaptic plasticity in mice with a spontaneous deletion in the ubiquitin C-terminal hydrolase L1 gene

Mikako Sakurai,[1,*] Masayuki Sekiguchi,[1,2,*] Ko Zushida,[1,2] Kazuyuki Yamada,[3] Satoshi Nagamine,[1] Tomohiro Kabuta[1] and Keiji Wada[1,2]
[1]Department of Degenerative Neurological Diseases, National Institute of Neuroscience, National Center of Neurology and Psychiatry, 4-1-1 Ogawahigashi, Kodaira, Tokyo 187–8502, Japan
[2]CREST, Japan Science and Technology Agency, Kawaguchi, Saitama 322–0012, Japan
[3]Support Unit for Animal Experiments, Brain Science Institute, RIKEN, 2–1 Hirosawa, Wako, Saitama 351–0198, Japan

Keywords: Alzheimer's disease, CREB, hippocampus, LTP, transcription

Abstract

Overexpression of ubiquitin C-terminal hydrolase L1 (UCH-L1) in mice rescues amyloid β-protein-induced decreases in synaptic plasticity and memory. However, the physiological role of UCH-L1 in the brain is not fully understood. In the present study, we investigated the role of UCH-L1 in the brain by utilizing gracile axonal dystrophy (*gad*) mice with a spontaneous deletion in the gene *Uch-l1* as a loss-of-function model. Although *gad* mice exhibit motor paresis beginning at ~ 12 weeks of age, it is possible to analyse their brain phenotypes at a younger age when no motor paresis is evident. Maintenance of memory in a passive avoidance test and exploratory behaviour in an open field test were reduced in 6-week-old *gad* mice. The maintenance of theta-burst stimulation-induced long-term potentiation (LTP) of field synaptic responses from Schaffer collaterals to CA1 pyramidal cells in hippocampal slices was also impaired in *gad* mice. The LTP in *gad* mice was insensitive to actinomycin D, suggesting that a transcription-dependent component of the LTP is impaired. Phosphorylation of cyclic AMP response element binding protein (CREB) in the CA1 region of hippocampal slices from *gad* mice occurred earlier than in the slices from wild-type mice and was transient, suggesting that CREB phosphorylation is altered in *gad* mice. These results suggest that memory in passive avoidance learning, exploratory behaviour and hippocampal CA1 LTP are reduced in *gad* mice. We propose that UCH-L1-mediated maintenance of the temporal integrity and persistence of CREB phosphorylation underlies these impairments.

Introduction

Ubiquitin C-terminal hydrolase L1 (UCH-L1) is a deubiquitinating enzyme (Wilkinson *et al.*, 1989) that is exclusively expressed in the brain and testis, and its expression is neuron-specific in the brain (Wilkinson *et al.*, 1989). Several lines of evidence suggest that UCH-L1 is involved in idiopathic Alzheimer's disease (AD) and Parkinson's disease (PD): (i) UCH-L1 is down-regulated in idiopathic AD and PD (Choi *et al.*, 2004), and in an AD model mouse (Gong *et al.*, 2006); and (ii) UCH-L1 is oxidatively modified in AD brains (Castegna *et al.*, 2002). Substitution of tyrosine for serine at codon 18 (S18Y polymorphism) in the *Uch-l1* gene exerts a protective effect against sporadic AD (Xue & Jia, 2006) and PD (Maraganore *et al.*, 1999). Furthermore, substitution of methionine for isoleucine at codon 93 (I93M mutation) reduces hydrolase activity of UCH-L1 and is linked to a rare autosomal dominant form of familial PD in a German family (Leroy *et al.*, 1998). Although these findings point to a role for UCH-L1 in AD and PD, the physiological role of UCH-L1 in the normal mammalian brain is not fully understood.

UCH-L1 has multiple functions *in vitro*. UCH-L1 removes small adducts or unfolded polypeptides from ubiquitin's C-terminus via hydrolysis (Larsen *et al.*, 1998). In addition, UCH-L1 has ubiquitin-ligase activity on α-synuclein-ubiquitin conjugates (Liu *et al.*, 2002). Apart from enzymatic activity, UCH-L1 acts as a stabilizer of monoubiquitin (Osaka *et al.*, 2003). UCH-L1 is thought to be a therapeutic target for AD; specifically, overexpression of UCH-L1 rescues amyloid β-protein (Aβ)-induced decreases in synaptic plasticity and contextual memory in mice (Gong *et al.*, 2006). Pharmacological suppression of UCH-L1 hydrolase activity (by 70%) is associated with impairment of synaptic transmission, tetanus-induced long-term potentiation (LTP) in the hippocampal CA1 field, and contextual fear memory in mice (Gong *et al.*, 2006). The nonmammalian Aplysia UCH has been identified as an immediate–early gene essential for long-term synaptic facilitation in the nervous system (Hedge *et al.*, 1997).

The aim of the present study was to further characterize the role of UCH-L1 in the mammalian brain. To this end, we utilized the UCH-L1-deficient *gracile axonal dystrophy* (*gad*) mouse, which is a spontaneous mutant with an in-frame deletion in exons 7 and 8 of *Uch-l1* (Saigoh *et al.*, 1999). Expression of the UCH-L1 protein is

Correspondence: Dr Keiji Wada, [1]Department of Degenerative Neurological Diseases, as above.
E-mail: wada@ncnp.go.jp

*M. Sakurai and M. Sekiguchi contributed equally to this study

Received 12 July 2007, revised 10 December 2007, accepted 12 December 2007

© The Authors (2008). Journal Compilation © Federation of European Neuroscience Societies and Blackwell Publishing Ltd

undetectable in the central nervous system of *gad* mice (Osaka *et al.*, 2003). In addition, recent analysis in our laboratory suggests that truncated products from the mutant *Uch-l1* are not detected in the *gad* mouse brain (T. Kabuta, unpublished observation). Although *gad* mice exhibit motor paresis beginning at ~12 weeks of age due to axonal degeneration of spinal cord neurons and subsequent degeneration of the spinocerebellar tract (Kikuchi *et al.*, 1990), it is possible to analyse the brain phenotypes of *gad* mice at younger ages when no motor paresis is evident. We found that memory in passive avoidance learning, exploratory behaviour and hippocampal synaptic plasticity are reduced in young *gad* mice (6 weeks of age).

Materials and Methods

Animals

Gad mice were bred at the Experimental Animal Center of the National Institute of Neuroscience, National Center of Neurology and Psychiatry, Tokyo. The original genetic background of *gad* mice was a hybrid of the CBA and RFM strains (Kikuchi *et al.*, 1990). However, *gad* mice were backcrossed to C57BL/6J strain mice 6–18 times before use in the present study. Six-week-old male *gad* mice and wild-type mice generated from heterozygous *gad* mating pairs were used for the experiments. Genotyping was carried out using PCR with the following three primers:

F1, 5′- agcttggagcctgtggtttcaactc-3′;
R1, 5′-tggcagcatcctgaaaaggagaggtg-3′;
R2, 5′-tacagatggccgtccacgttgttga-3′

The reaction conditions were 35 cycles of 94 °C for 20 s, 60 °C for 30 s and 72 °C for 60 s. The wild-type allele produced an 891-bp PCR product, and the *gad* allele produced a 446-bp PCR product. Three to five mice were housed per cage under controlled temperature (25 ± 1 °C) and lighting (12-h light–dark cycle) conditions and provided with food and water *ad libitum*. The experiments were performed in strict accordance with the National Institute of Neuroscience's regulations for animal experimentation, and were approved by the Animal Investigation Committee of the Institute.

Histology

Hematoxylin and eosin (H&E) staining was performed as reported (Kikuchi *et al.*, 1990). For immunohistochemistry, 4-μm-thick paraffin sections were de-paraffinized and pretreated in a microwave oven with 10 mM citrate–NaOH buffer (pH 6.0). After blocking with phosphate-buffered saline containing 1% heat-inactivated normal goat serum and 0.1% [(v/v)] Triton X-100, slides were incubated with an anti-Aβ monoclonal antibody (clone 4G8, 1 : 100 dilution; Signet Laboratories, Dedham, MA, USA) or an antisynaptophysin monoclonal antibody (MAB5258, 1 : 500 dilution; Chemicon, Temecula, CA, USA) and then with Envision+horseradish peroxidase–labelled anti-mouse IgG (DakoCytomation Inc., Carpinteria, CA, USA). Chromogenic detection was performed using the DAB Substrate kit (DakoCytomation Inc.). Sections were examined with a BX51 microscope (Olympus).

Behavioural tests

One-trial passive avoidance tests were performed as described (Yamada *et al.*, 2003). Briefly, a single mouse was introduced into a light compartment of a light–dark box (Muromachi-kikai, Tokyo, Japan). During habituation, mice were allowed to freely explore the box for 5 min with the sliding door between the light and dark compartments open; after that, the mice were returned to their home cage. For conditioning, which was carried out 2 h after habituation, the mice were introduced into the light compartment, the sliding door was closed when both hindlimbs had entered into the dark box, and an electrical footshock was delivered via the floor grid in the dark compartment (300 μA, 3 s duration, using a shock generator–scrambler; Muromachi-kikai). The mice were left in the light–dark box for 5 min and then returned to their home cage. Tests were carried out 2 or 24 h after the conditioning by re-introducing the mice into the light compartment of the light–dark box. The latency time for mice to enter the dark compartment was measured (light–dark latency, with a 5 min cut-off). The tests at 2 and 24 h postconditioning were carried out using different groups of mice.

The pain sensitivity of mice was tested as described (Yamada *et al.*, 2003). Briefly, a series of footshocks of ascending (20, 40, 60, 80, 100 and 130 μA, 1 s duration) and descending (130, 100, 80, 60, 40 and 20 μA, 1 s duration) current were serially delivered to the mice via the floor grid. The input current that induced hindlimb withdraw was recorded. The interfootshock interval was 15 s. This trial was performed six times, and the data were averaged.

Open field tests were performed as we described (Zushida *et al.*, 2007). Briefly, the test was carried out in an arena (a 50 × 50 cm white field surrounded by a 40-cm-high white wall, illuminated with 80 lx) placed in a soundproof box. Mice were placed at the periphery of the arena, and for 5 min the behaviour of the mice was recorded using a digital video camera linked to a computer. Locomotor activity was calculated from this record by Image OF (O'Hara & Co., Ltd, Tokyo, Japan), modified software based on the public domain NIH Image program. Rearing was manually counted.

The light–dark box test was performed as described (Yamada *et al.*, 2002). Briefly, mice were placed into the dark compartment of the light–dark box and were allowed to explore both sides of the light–dark box for 5 min. During these 5 min, three parameters were measured: latency to enter the light compartment, number of entries into the light compartment, and duration in the light compartment.

Electrophysiology

Each 6-week-old male mouse was anaesthetized with halothane, and the brain was quickly removed. Preparation of hippocampal slices for electrophysiology was carried out as reported (Takamatsu *et al.*, 2005; Zushida *et al.*, 2007). Briefly, the hippocampus was isolated from the brain, and transverse slices (400 μm thick) were prepared using a Vibratome 3000 microtome (Vibratome Company, St Louis, MO, USA) in a sucrose-based cutting solution (in mM: sucrose, 234; KCl, 25; NaH_2PO_4, 1.25; $MgSO_4$, 10; $NaHCO_3$, 26; glucose, 11; and $CaCl_2$, 0.5). The slices were maintained at room temperature in artificial cerebrospinal fluid (ACSF; in mM: NaCl, 125; KCl, 4.4; $MgSO_4$, 1.5; NaH_2PO_4, 1.0; $NaHCO_3$, 26; glucose, 10; and $CaCl_2$, 2.5; pH 7.4, 290–300 mOsm/L) continuously bubbled with 95% O_2 and 5% CO_2. A slice was then transferred to the recording chamber and was continuously superfused at 3 mL/min with ACSF maintained at 28–32 °C.

Extracellular field recordings were carried out as reported (Takamatsu *et al.*, 2005). Briefly, field excitatory postsynaptic potentials (fEPSPs) were recorded from CA1 stratum radiatum of the hippocampus using a glass micropipette (1–2 MΩ) filled with ACSF. The electrical signals were amplified using a MultiClamp 700B amplifier (Axon Instruments, Foster City, CA, USA), filtered at 10 kHz, digitized at 10 kHz and acquired with Clampex (ver. 9.2). A bipolar stainless steel stimulating electrode was placed in stratum radiatum at the border between CA2 and CA3 to stimulate the Schaffer collateral pathway. The pulse intensity was adjusted to give 40% of the maximum amplitude in all experiments. Stimulation was carried out in

© The Authors (2008). Journal Compilation © Federation of European Neuroscience Societies and Blackwell Publishing Ltd

constant current mode (100 μs duration). The fEPSPs for which the 40% amplitude was > 1 mV were used for data analysis. The strength of synaptic transmission was determined by measuring the rising phase (20–60%) of the fEPSP slope. The average fEPSP slope during the 10 min prior to LTP induction was taken as the baseline, and all values were normalized to this baseline. The baseline stimulation frequency was 0.033 Hz. LTP was induced by applying theta-burst stimulation (TBS; 15 bursts of four pulses at 100 Hz, delivered at an interburst interval of 200 ms) or tetanic stimulation (100 Hz, 1 s, three times with a 20 s interval). Paired-pulse facilitation was induced by delivering two consecutive pulses with a 20-, 50-, 100-, 200- or 400-ms interpulse interval.

Somatic whole-cell patch-clamp recordings were made with a MultiClamp 700B amplifier (Zushida *et al.*, 2007). Pyramidal-shaped neurons in the CA1 pyramidal layer visually identified with differential contrast video microscopy (Hamamatsu Photonics, Hamamatsu, Japan) on an upright microscope (Axioscope, Zeiss, Oberkochen, Germany) were selected for recording. The patch electrodes were 6–10 MΩ when filled with a solution containing (in mM): K gluconate, 132; KCl, 3; HEPES, 10; EGTA, 0.5; $MgCl_2$, 1; sodium phosphocreatine, 12; ATP·Mg, 3; and GTP, 0.5 (pH 7.4 with KOH, 285–290 mOsm/L). We used this solution when measuring membrane potential and input resistance. The input resistance was calculated by injecting a square current pulse (−10 pA) in current-clamp mode. For comparison of synaptic currents at −70 and +40 mV, an internal solution containing (in mM): CsOH, 105; CsCl, 30; HEPES, 10; EGTA, 0.5; $MgCl_2$, 1; sodium phosphocreatine, 12; ATP·Mg, 3; and GTP, 0.5 (pH 7.3 with gluconic acid, 295 mOsm/L) was used. The signal was digitized at one point per 50 μs and stored using Clampex. The resting membrane potential of the cells used in the analysis ranged from −57 to −67 mV, and the series resistance was 3–20 MΩ. Synaptic responses were elicited by electrical stimulation as described for extracellular recording. The pulse intensity was adjusted to elicit excitatory postsynaptic potentials (EPSPs) 40% of the amplitude required for action potential generation in current-clamp mode.

All chemicals and drugs used for electrophysiology were purchased from Sigma with the exception of actinomycin D, which was obtained from Wako Pure Chemicals (Tokyo, Japan). Actinomycin D was dissolved in dimethylsulfoxide at 40 mM, added to ACSF just prior to application at 40 μM, and bath-applied with perfusion. Therefore, the final dimethylsulfoxide concentration was 0.1%.

Western blotting

For analysis of Aβ, the hippocampus was isolated from the brain and snap-frozen in liquid nitrogen. The tissue was homogenized in ice-cold buffer (Tris-HCl, 50 mM; NaCl, 150 mM; EDTA, 5 mM; and Triton X-100, 1%; pH 7.5) containing proteinase inhibitors (Complete, EDTA-free; Roche Applied Science, Indianapolis, IN, USA) and phosphatase inhibitors (Halt phosphatase inhibitor cocktail; Pierce, Rockford, IL, USA), and the homogenate was subjected to SDS-PAGE. Western blotting was carried out as we reported (Kabuta *et al.*, 2006) using anti-Aβ (clone 4G8; Signet Laboratories), anti-UCH-L1 (UltraClone Ltd, UK) and anti-β-actin (Sigma) antibodies. Briefly, immunoreactive signals were visualized with SuperSignal West Femto maximum sensitivity substrate (Pierce) or SuperSignal West Dura extended duration substrate (Pierce) and detected with a chemiluminescence imaging system (FluorChem; Alpha Innotech, San Leandro, CA, USA). Human Aβ 1–42 from Peptide Institute, Inc., Osaka, Japan served as the positive control.

Following extracellular recording, hippocampal slices were retrieved for Western blotting. The dentate gyrus and CA3 region of the slices were cut off, and the remaining CA1 region was snap-frozen in liquid nitrogen. Tissue samples from each slice were homogenized in the same buffer as used for the Aβ analysis, and the homogenate was subjected to SDS-PAGE. The antibodies used were anti-phospho-CREB (serine 133), anti-CREB (Cell Signalling Technology, Inc., Danvers, MA, USA), anti-cAMP-dependent protein kinase (protein kinase A; PKA) regulatory subunit RIα and RIIα (BD Biosciences, San Jose, CA, USA), anti-UCH-L1 (UltraClone Ltd) and anti-β-actin (Sigma). Immunoreactive signals were visualized as described for the Aβ analysis. The signal intensity was quantified by densitometry using FluoChem software (Alpha Innnotech).

Data and statistical analysis

Numerical data are expressed as the mean ± SEM. The two-tailed Student's *t*-test was used for comparison between wild-type mice and *gad* mice. Repeated-measures one-way ANOVA was used to analyse whether footshock and exposure to an open field arena had significant effects within a genotype in passive avoidance and open field tests, respectively. ANOVA with the Bonferroni–Dunn test was used to compare the three data groups in the pCREB analysis.

Results

Structural abnormalities were not detected in the cerebrum and hippocampus of young gad mice

Before behavioural analysis, we first examined whether there were any histological abnormalities in the cerebral cortex and hippocampus of 6-week-old *gad* mice. It has been reported that the thalamus is not impaired in *gad* mice (Kikuchi *et al.*, 1990), but there is no report on the cortex and limbic system. Figure 1A–D shows H&E staining of coronal brain sections (at bregma level −1.7 mm) from a wild-type mouse (Fig. 1A and C) and *gad* mouse (Fig. 1B and D; 6 weeks of age). We could not detect any visible abnormalities, such as atrophy or lack of cells, in the hippocampus or cortex of *gad* mice ($n = 2$). One anatomical characteristic of *gad* mice is spheroid structures in the medulla and spinal cord that are thought to be degenerating axons (Kikuchi *et al.*, 1990). We did not find this aberration in the hippocampus or cortex of *gad* mice (Fig. 1A–D). We also examined other brain regions in sections cut at bregma levels 2.5, 1.0, −3.0 and −6.0 mm, and no outstanding abnormalities were evident in the *gad* mice (data not shown). In addition, we carried out immunohistochemical staining using antisynaptophysin. This antibody stains presynaptic sites and thus the staining pattern would be expected to be different in *gad* mice if there was noticeable axonal degeneration. Typical punctate synaptophysin staining was obtained in both wild-type (Fig. 1E and G) and *gad* (Fig. 1F and H) mice. We could not detect any visible differences in the staining of the hippocampus between wild-type and *gad* mice. These results suggest that structural impairment of the brain at a macroanatomical level is not evident in 6-week-old *gad* mice.

Axonal degeneration promotes accumulation of Aβ in the medulla and spinal cord of *gad* mice (Ichihara *et al.*, 1995). Consistent with the lack of spheroid structures in the cortex and hippocampus, we did not find abnormal accumulation of Aβ in these brain regions in *gad* mice up to 12 weeks of age (immunohistochemical analysis using an antibody to Aβ; data not shown). Furthermore, we examined nonfibrillar Aβ by Western blotting. We could not detect any significant bands in the samples from wild-type and *gad* mouse hippocampi when blotting with anti-Aβ (Fig. 1I, upper panel). Authentic human Aβ (the right two lanes, a positive control) blotted

© The Authors (2008). Journal Compilation © Federation of European Neuroscience Societies and Blackwell Publishing Ltd

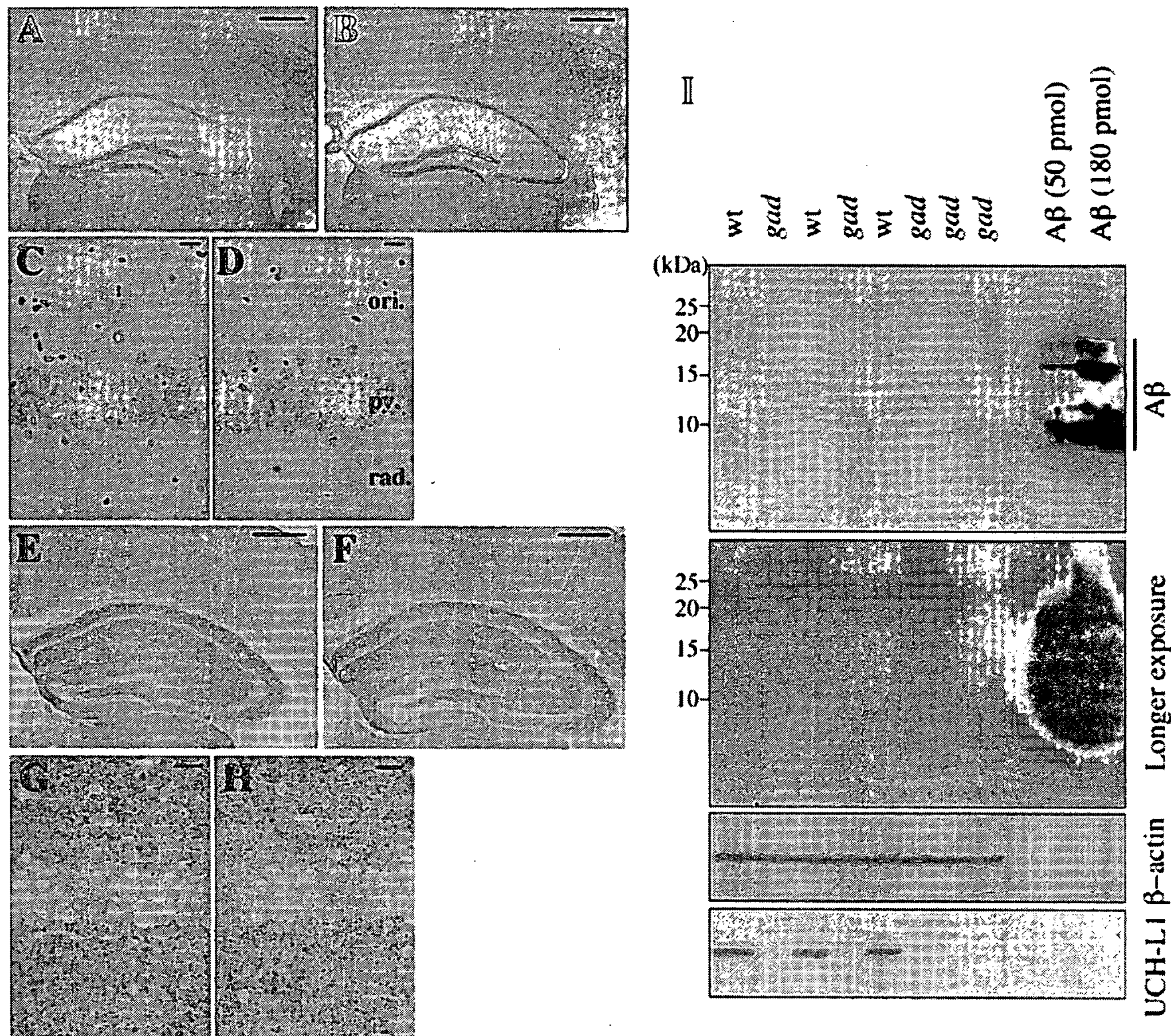

FIG. 1. Six-week-old *gad* mice have normal brain histology. (A–D) H&E staining of coronal brain sections from (A and C) a 6-week-old wild-type (wt) mouse and (B and D) a 6-week-old *gad* mouse. (C and D) A higher magnification of the hippocampal CA1 field. ori., stratum oriens; py., pyramidal cell layer; rad., stratum radiatum. (E–H) Synaptophysin immunohistochemistry in coronal brain sections from a six-week-old wt mouse (E and G) and a six-week-old *gad* mouse (F and H). (G and H) A higher magnification of the hippocampal CA1 field. (I) Western blotting of samples prepared from the hippocampi of three wt and five *gad* mice. Antibodies against Aβ, β-actin and UCH-L1 were used. Authentic Aβ was used as a positive control. A short exposure is shown in the upper panel; a longer exposure is shown below. Molecular size markers (kDa) are shown on the left. Scale bars, 500 μm (A, B, E and F), 20 μm (C, D, G and H).

densely on the same membrane. After a longer exposure (Fig. 1I) we could detect certain bands, but there was no band that was significantly increased in *gad* mice compared with wild-type mice. Blots using antiβ-actin and anti-UCH-L1 were carried out to confirm the sample load and genotype, respectively (Fig. 1I).

Lack of UCH-L1 in mice impaired memory maintenance in the passive avoidance test and exploratory behaviour for a novel environment

Next, we examined whether lack of UCH-L1 had a detectable impact on mouse behaviour. For this purpose, we carried out one-trial passive avoidance tests. Figure 2A shows the performance of wild-type and *gad* mice in this test. After habituation to the light–dark box, mice were conditioned with an electrical footshock when they entered the dark compartment. We then tested their ability to avoid the dark compartment 24 h after the conditioning footshock. The footshock significantly prolonged the light–dark latency in wild-type mice (comparison of the conditioning and test sessions $P = 0.003$, $F = 14.6$, $n = 12$; repeated-measures ANOVA). In contrast, the light–dark latency was not significantly affected in *gad* mice (comparison of the conditioning and test sessions using repeated-measures ANOVA, $P = 0.2437$, $F = 1.556$, $n = 10$), suggesting that memory function, as assessed by this test, is impaired in *gad* mice. In

© The Authors (2008). Journal Compilation © Federation of European Neuroscience Societies and Blackwell Publishing Ltd

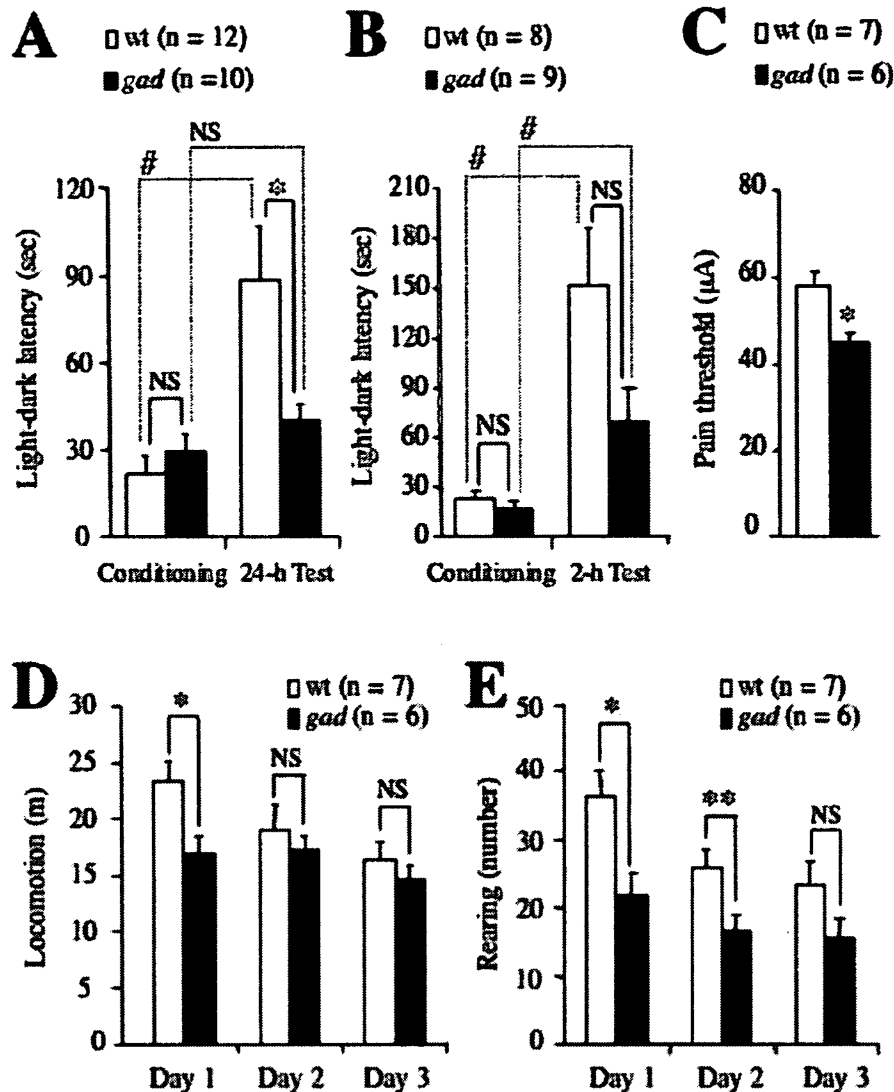

FIG. 2. Impairment of memory maintenance and exploratory behaviour in *gad* mice. (A and B) Light–dark latency of mice in a one-trial passive avoidance test. After habituation to a light–dark box, mice were conditioned with an electrical footshock when they entered the dark compartment (Conditioning). At (A) 24 h or (B) 2 h after the footshock, the mice were reintroduced into the light–dark box and the time for mice to enter the dark compartment (light–dark latency) was measured (Test). $^{*}P = 0.028$; NS, not significant; two-tailed Student's t-test (solid lines). $^{\#}P < 0.020$; NS, not significant, repeated-measures one-way ANOVA (dotted lines). (C) Pain sensitivity of the mice was measured by applying a series of electrical footshocks. $^{*}P = 0.002$, two-tailed Student's t-test. (D) Locomotor activity of wild-type and *gad* mice in an open field arena. The mice were introduced into the arena for the first time on day 1. $^{*}P = 0.023$, two-tailed Student's t-test. (E) Rearing frequency of wild-type and *gad* mice in an open field arena. $^{*}P = 0.014$, $^{**}P = 0.021$; two-tailed Student's t-test.

addition, the light–dark latency in the 24-h test session differed significantly between the wild-type and *gad* mice ($P = 0.028$; two-tailed Student's t-test). We next conducted a test session 2 h after conditioning to test whether learning ability was impaired in *gad* mice shortly after conditioning. In the test 2 h after conditioning (Fig. 2B), the footshock had a significant effect on the light–dark latency in both wild-type and *gad* mice ($P = 0.0147$, $F = 10.356$, $n = 8$ for wild-type mice; $P = 0.0199$, $F = 8.407$, $n = 9$ for *gad* mice; repeated-measures ANOVA). The average latency in the 2-h test session did not differ significantly between the wild-type and *gad* mice ($P = 0.074$; two-tailed Student's t-test). These results suggest that *gad* mice are able to learn but maintenance of memory is reduced. Because the pain sensitivity of *gad* mice was greater than that of wild-type mice (Fig. 2C; $P = 0.002$ with two-tailed Student's t-test), the footshock used for conditioning was indeed an aversive stimulus in *gad* mice.

Next, we carried out the open field test. Mice were exposed to an open field arena for the first time on day 1 (Fig. 2D). The wild-type mice explored the novel environment and showed high locomotor activity (Fig. 2D). Locomotor activity was reduced upon re-exposure of wild-type mice to the same arena on days 2 and 3 because they remembered the arena, and thus the novelty was reduced ($P = 0.024$, $F = 12.928$, $n = 7$; repeated-measures ANOVA). In contrast, locomotor activity was not significantly decreased in *gad* mice ($P = 0.392$, $F = 1.030$, $n = 6$; repeated-measures ANOVA). The locomotor activity on day 1 differed significantly between wild-type and *gad* mice ($P = 0.023$; two-tailed Student's t-test), but the activity on day 2 or 3 did not ($P = 0.500$ and 0.446 for days 2 and

© The Authors (2008). Journal Compilation © Federation of European Neuroscience Societies and Blackwell Publishing Ltd

3, respectively). To determine whether the difference in locomotor activity on day 1 was due to reduced exploratory behaviour in *gad* mice, we measured the frequency of rearing, a typical exploratory behaviour (Lever *et al.*, 2006; Fig. 2E). Similar to locomotor activity, upon re-exposure rearing frequency decreased in wild-type mice ($P = 0.009$, $F = 14.257$, $n = 7$; repeated-measures ANOVA) but not in *gad* mice ($P = 0.131$, $F = 2.503$, $n = 6$; repeated-measures ANOVA). The rearing frequency on days 1 and 2 differed significantly between wild-type and *gad* mice ($P = 0.014$ and 0.021 for days 1 and 2, respectively; two-tailed Student's t-test), but the activity on day 3 did not ($P = 0.093$). These results suggest that exploratory behaviour in a novel environment is reduced in *gad* mice.

Although these data apparently suggest that memory in passive avoidance learning and exploratory behaviour are reduced in young *gad* mice, there is a possibility that the anxiety state of *gad* mice is altered. Alterations in the anxiety state can affect memory (Bouton *et al.*, 1990) and the response to novel environments. To measure anxiety, we performed a light–dark box test. In this test, mice usually avoid the light compartment. Therefore, the level of anxiety can be measured as the latency to move into the light compartment and the duration of time in the light compartment (Yamada *et al.*, 2002). Because the passive avoidance test also utilizes these properties, performance in the light–dark test is important for interpreting the results from the passive avoidance test. The time required for the mice to step into the light compartment when introduced into the dark compartment (dark-light latency; Fig. 3A), the time the mice spent in the light compartment (Fig. 3A) and the number of times the mice crossed between compartments (Fig. 3B) did not differ significantly between wild-type and *gad* mice ($P = 0.834$, 0.417 and 0.109, respectively; two-tailed Student's t-test). These results suggest that anxiety state, as assessed by this test, was not obviously altered in *gad* mice. Therefore we concluded that the impairments in passive avoidance learning and exploratory behaviour were not due to alterations in the anxiety state.

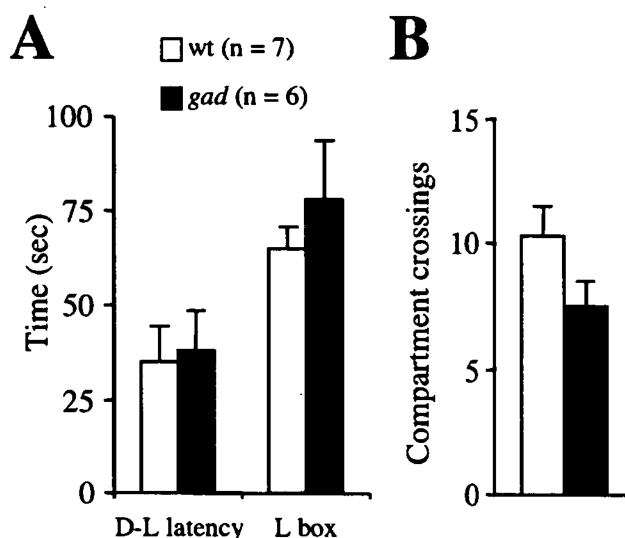

FIG. 3. Wild-type and *gad* mice performed similarly in the light–dark box test. (A) Dark–light (D-L) latency and duration of time in the light compartment (L box). (B) Number of crossings between the two compartments.

Impairment of a transcription-dependent component of LTP in gad mice

We tested whether the lack of UCH-L1 affects neuronal function by measuring LTP at Schaffer collateral synapses onto CA1 pyramidal neurons in hippocampal slice preparations. LTP is believed to be a synaptic mechanism underlying memory and learning (Bliss & Collingridge, 1993). The CA1 synapse was selected because this brain region is involved in spatial memory (Morris *et al.*, 1982) and passive avoidance memory (Bevilaqua *et al.*, 1997; Impey *et al.*, 1998). In wild-type slices, TBS induced robust LTP at CA1 synapses (Fig. 4A), as reported for C57BL/6J mice (Nguyen & Kandel, 1997; Nguyen *et al.*, 2000). In contrast, TBS-induced LTP was attenuated in *gad* mice beginning ~ 20 min post-TBS (Fig. 4A). At 45 min post-TBS, normalized synaptic responses were significantly greater in wild-type slices (1.87 ± 0.08, $n = 7$) than in *gad* slices (1.36 ± 0.07, $n = 6$; $P = 0.001$, two-tailed Student's t-test). Impairment of LTP in *gad* mice depended on the stimulation pattern. Tetanus-induced LTP was identical in wild-type and *gad* mice (Fig. 4B; normalized fEPSP slopes at 45 min post-tetanus: wild-type, 1.81 ± 0.16, $n = 5$; *gad*, 1.86 ± 0.25, $n = 5$).

Stimulus–output curves (Fig. 5A) and paired-pulse facilitation (Fig. 5B) of CA1 synapses were essentially identical in wild-type and *gad* mice. The latter result suggests that a postsynaptic, rather than presynaptic, mechanism is involved in impairment of TBS-induced LTP in *gad* mice. LTP at this synapse is dependent on postsynaptic NMDA receptors (Harris *et al.*, 1984; Larson & Lynch, 1988). Therefore, we tested whether NMDA receptor activity was reduced in *gad* mice using patch-clamp recordings. For this purpose, we recorded Schaffer collateral–CA1 synaptic responses in neurons voltage-clamped to −70 and +40 mV in the presence of picrotoxin (50 μM). The amplitude of the synaptic response recorded at +40 mV at 100 ms poststimulation was normalized to the peak amplitude of the response at −70 mV to estimate the ratio of NMDA-mediated to non-NMDA-mediated currents (Fig. 5D). Because superfusion of the slices with picrotoxin frequently elicited epileptiform activity (data not shown), three to five synaptic responses without epileptiform activity were selected and averaged. The ratio was identical in wild-type and *gad* mice (0.45 ± 0.05, $n = 5$ and 0.43 ± 0.05, $n = 7$ for wild-type and *gad* mice, respectively; two-tailed Student's t-test). Therefore, attenuation of synaptic NMDA receptor activity does not account for reduced LTP in *gad* mice. Resting membrane potential and input resistance of CA1 pyramidal neurons did not differ substantially between wild-type and *gad* mice [resting membrane potential, -60.1 ± 0.4 mV for wild-type mice ($n = 20$) and -60.0 ± 0.6 mV for *gad* mice ($n = 20$); input resistance, 163 ± 9.6 for wild-type mice ($n = 16$) and 175 ± 10.8 for *gad* mice ($n = 13$); results obtained from the records using potassium-gluconate pipette solution].

CA1 LTP is composed of early and late temporal phases (Nguyen *et al.*, 1994; Abel *et al.*, 1997; Nguyen & Kandel, 1997). The former is induced mainly by an increase in the number of AMPA-type glutamate receptors at the synapse (reviewed in Malinow & Malenka, 2002) whereas the latter is induced by new protein synthesis from transcription of new mRNA (Nguyen *et al.*, 1994) and/or local protein synthesis from previously expressed mRNA (Bradshaw *et al.*, 2003). Because no obvious changes in the early phase of LTP (up to ~ 20 min post-TBS) were observed in *gad* mice, we tested whether the late phase is occluded in *gad* mice. For this purpose, we applied actinomycin D, a transcription inhibitor, to the slices and compared suppression of TBS-induced LTP in wild-type and *gad* mice. In wild-type mice, the maintenance of TBS-induced LTP was suppressed by actinomycin D (Fig. 6A). The normalized fEPSP slope at 45 min

© The Authors (2008). Journal Compilation © Federation of European Neuroscience Societies and Blackwell Publishing Ltd